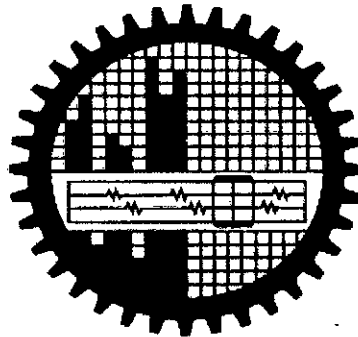# Dispersion Analysis of Photonic Crystal Fibers Considering Thermal and External Stress Effects

By

Md. Afzal Hossain

Student ID: 100706245P

DEPARTMENT OF ELECTRICAL AND ELECTRONIC ENGINEERING

BANGLADESH UNIVERSITY OF ENGINEERING AND TECHNOLOGY

Dhaka-1000, Bangladesh

July 2009

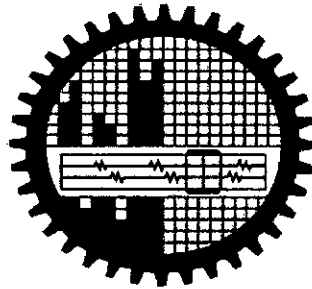# Dispersion Analysis of Photonic Crystal Fibers Considering Thermal and External Stress Effects

A thesis submitted to
the Department of Electrical and Electronic Engineering,
Bangladesh University of Engineering and Technology
in partial fulfillment of the requirements
for the degree of

## MASTER OF SCIENCE IN ELECTRICAL AND ELECTRONIC ENGINEERING
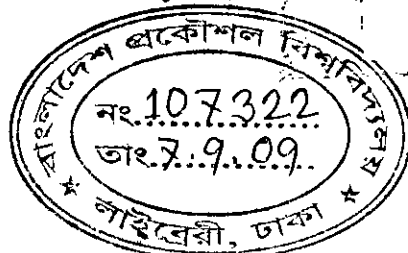
By

Md. Afzal Hossain

Student ID: 100706245P

Department of Electrical and Electronic Engineering

Bangladesh University of Engineering and Technology (BUET)
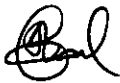
Dhaka-1000, Bangladesh

July 28, 2009

#107322#

# DECLARATION

It is hereby declared that this thesis or any part of it has not been submitted elsewhere for the award of any degree or diploma.
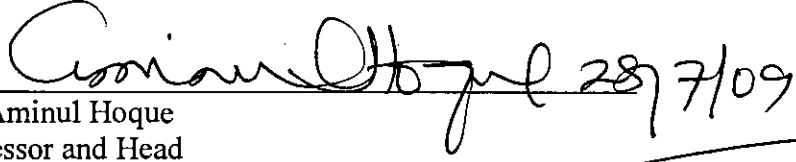
Signature of the student

------------------------------------

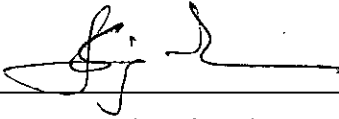(Md. Afzal Hossain)
Student ID: 100706245P
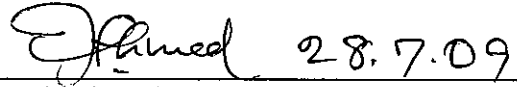
# APPROVAL CERTIFICATE

The thesis titled "DISPERSION ANALYSIS OF PHOTONIC CRYSTAL FIBERS CONSIDERING THERMAL AND EXTERNAL STRESS EFFECTS" submitted by Md. Afzal Hossain, Student ID : 100706245P, Session: October 2007 has been accepted as satisfactory in partial fulfillment of the requirement for the degree of Master of Science in Electrical and Electronic Engineering on 28 July, 2009.

## BOARD OF EXAMINERS

1. _Signature_                                                      Chairman
                                                                    (Supervisor)

Dr. Md. Shah Alam
Associate Professor
Department of EEE, BUET
Dhaka -1000, Bangladesh.

2. _Signature_ 28/7/09                                              Member
                                                                    (Ex-Officio)
Dr. Aminul Hoque
Professor and Head
Department of EEE, BUET
Dhaka -1000, Bangladesh.

3. _Signature_                                                      Member

Dr. Satya Prasad Majumder
Professor
Department of EEE, BUET
Dhaka -1000, Bangladesh.

4. _Signature_ 28. 7. 09                                            Member
                                                                    (External)
Dr. Farruk Ahmed
Professor
Department of Electrical Engg and Computer Science
North South University, Dhaka, Bangladesh.

# ACKNOWLEDGEMENT

At first, I must express my utmost gratefulness and sincerest thanks to the almighty Allah, the most gracious, the most merciful for giving me this opportunity to complete my research work and the thesis.

I would like to express my sincere appreciations and deepest gratitude to Dr. Md. Shah Alam Associate Professor, Dept of EEE, BUET, Dhaka, Bangladesh for his all out support, relentless endeavor and keen supervision throughout the thesis work. I am particularly indebt to him for timely guiding me by holding series of academic discussions and providing with all necessary information for the work. It is his inspiration, encouragement and untiring supervision that have enabled me to finish this work within the stipulated time. I am truly benefited of having the experience of doing research work with him.

I am grateful to Professor Dr. Aminul Hoque, Head of the department of Electrical and Electronic Engineering, BUET for rendering me all support and departmental assistance during my M.Sc study in BUET. He has allowed me to use the library, computer laboratory and all other facilities of the department at the time of requirements. I would like to convey my thanks to all faculty and other members of the department for their support during my research work.

Last but not the least, it would be unjust if I do not mention about the contribution of my family members who have always encouraged me and rendered their support to continue my studies and research work.

# ABSTRACT

Analysis of the effects of thermal and external stress on the properties of solid core Photonic Crystal Fiber (PCF) has been carried out in this research work, by using the finite element method (FEM). The PCF is modeled here using the COMSOL Multiphysics software, where structural mechanics module and electromagnetic module have been employed for carrying out the stress analysis and optical analysis, respectively. The external stress acting on the holey fiber induces a specific stress distribution in the fiber's cross section. This stress distribution causes isotropic fiber material to become birefringent. In the PCF, due to the external stress, the refractive index of the material changes due to the photoelastic effect. So, stress analysis has been carried out first using plane strain approximation to find the new anisotropic index of the fiber material when there is stress-optic effect associated with the PCF. Here, a simultaneous linear system of equations resulting from plane-strain approximation has been solved for nodal displacements. Finally, with the new refractive index of the fiber material, optical analysis has been carried out to obtain effective refractive index. Finally, different propagation properties, like, group birefringence, beat length, effective mode area, modal confinement, polarization mode dispersion, group velocity dispersion, etc. are determined and the effects of thermal and external stress on all theses properties have been discussed. Also, wavelength dependence and structural dependence of the propagation properties have been studied and presented in this work.

# Table of Contents

# Chapter 3: Stress Analysis of Photonic Crystal Fibers

# Chapter 4: Results and Discussions

# Chapter 5: Conclusion

# List of Figures

# List of Tables

# LIST OF ABBREVIATIONS

| | |
|---|---|
| DCF | Dispersion Compensating Fiber |
| GVD | Group Velocity Dispersion |
| PCF | Photonic Crystal Fiber |
| PMD | Polarization Mode Dispersion |
| PMF | Polarization Maintaining Fiber |
| GD | Group Delay |
| HiBi | Highly Birefringence |
| FEM | Finite Element Method |
| LPMF | Linear Polarization Maintaining Fiber |
| MOF | Microstructured Optical Fiber |
| MMF | Multi Mode Fiber |
| SMF | Single Mode Fiber |
| SMSP | Single Mode Single Polarization Fibers |
| FSM | Fundamental Space-Filling Mode |
| WiMAX | Worldwide Interoperability for Microwave Access |
| TE | Transverse Electric |
| TM | Transverse Magnetic |
| HF | Holey Fiber |

# CHAPTER 1

# Introduction
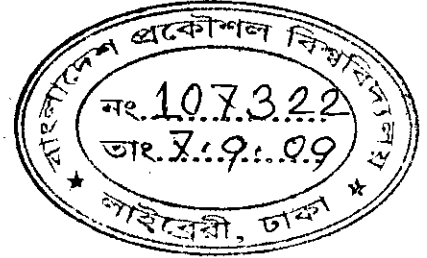
## 1.1 Photonic Crystal Fibers in Optical Fiber Communication Systems

Optical fibers have a very broad range of applications, where they serve many purposes, such as simply transporting light from a source to some other device, transmitting optically encoded data at enormously high speed, sensing temperature or strain in some environment, or generating and amplifying laser light. The most basic function of a fiber is to guide light, i.e., to keep light concentrated over longer propagation distances despite the natural tendency of light beams to diverge. In the simple step-index fiber, light guidance is achieved by creating a region with increased refractive index around the fiber axis, called the fiber core, which is surrounded by the cladding. The guiding effect explained as a result of total internal reflection: a light beam approaching the core - cladding interface from the core region is reflected provided that the incidence angle (measured against the normal direction) is sufficiently large. A very important concept in fiber optics is that of waveguide modes. Of highest interest are usually the guided modes, i. e., those modes which have significant intensity only in or near the core. Depending on the fiber design and the optical wavelength, some number of guided modes may exist, or only a single one, or even no guided mode at all. A fiber with only one guided mode is called a single-mode fiber, and multimode fibers support more than one guided modes. Both multi-mode and single-mode fibers are used in communications, with multi-mode fiber used mostly for short distances, and single-mode fiber used for longer distance links.

For glass optical fiber, the maximum transmission distance is limited by attenuation and also by dispersion, or spreading of optical pulses as they travel along the fiber. Single-mode fiber has no inter-modal dispersion as it supports only one transverse mode. But its performance is limited by chromatic dispersion, which occurs because the index of the glass is wavelength dependent, and light from optical transmitters has nonzero spectral width. Polarization mode dispersion limits the performance of single-mode systems. Dispersion limits the bandwidth of the fiber because the spreading optical pulse limits the rate that pulses can follow one another on the fiber and still be distinguishable at the receiver. Recent advances in optical communications technology have reduced signal degradation so far that no regeneration of the optical signal is needed over distances of hundreds of kilometers. This has reduced the cost of

optical networking, where the cost and reliability of repeaters are the key factors determining the performance of the whole cable system. Yet, it is a great concern for the researchers of the environment effect on the fiber, specifically the pressure effect on the fiber that can alter the birefringence properties or exert a provocation for higher polarization mode dispersion in the fiber. All these issues have drawn the attention of the scientists and researchers to innovate new types of materials or novel design of optical fibers from a single material.

In the recent years, there has been a significant interest among the researchers of fiber optic on photonic crystal fibers (PCF), which are also called microstructured optical fibers (MOFs) [1]. These PCFs are usually made of a single material, e.g., pure silica ($SiO_2$) or polymer formed by a central solid defect region surrounded by cladding consisting of a two dimensionally periodic array of multiple air holes in a regular triangular or rectangular lattice, where the air holes run along the length of the fiber. So far studies go, till now, there are mainly two types of PCFs–holey fibers and bandgap fibers. The core in PCF is a deliberate defect region, where there is a missing air hole in the centre in case of holey fibers, and the presence of a central air hole in case of bandgap fibers. Light confinement is explained by two different mechanisms: the index guiding effect; and photonic bandgap effect. Bandgap guidance has no analogue in conventional fibers and allows for novel features such as high confinement in a low-index core, even in air hole. The index guiding PCF confines light by total internal reflection like in conventional step-index fibers. The PCFs offer a number of unique and useful properties, such as a wide single-mode wavelength range, anomalous group velocity dispersion (GVD) which are unachievable in traditional silica glass fibers. Propagation properties in unstressed PCF have been addressed widely using different analysis techniques and tools [7]-[12]. Recently, the influence of lateral force on the birefringence and other properties of PCF has been investigated [12]. However, the propagation properties, like, birefringence, effective mode area, GVD and PMD etc. of PCF under external uniform stress have not yet been reported upon. Thus, it is important to study the effects of external stress on the dispersion properties of PCFs as the demand of PCFs is increasing day by day in various fields of applications. In our research work, the effects of uniform external stress including the thermal stress on the properties of PCF have been studied and analyzed. Under the external stress conditions, birefringence, modal confinement, and dispersions have been determined and presented in graphical forms. In the process, the influence of the geometrical structure (core size, number of the layer of air hole rings etc.) on the leading properties of the PCF has also been discussed in the work.

2

## 1.2    Review of Literature

Conventional optical fibers rely on total internal reflection to guide light. The simplest optical fiber, the step index fiber consists of a dielectric core with refractive index $n_{co}$ surrounded by another dielectric (called cladding) with refractive index $n_{CL}$. If the refractive index of the core is higher than that of the cladding, light propagating in the core in the direction of propagation and reaching the core/cladding interface is totally reflected back into the core as soon as the angle between the direction of propagation and the core/cladding interface is small enough [1]-[4]. Photonic crystal fibers guide light by corralling it within a periodic array of microscopic air holes that run along the entire fiber length. Because of having the ability to overcome the limitations of conventional fiber optics-for example, by permitting low-loss guidance of light in a hollow core (Bandgap), PCFs have immense potential of technological and scientific applications in various disciplines [5]-[6]. Losses in conventional silica fibers increase towards shorter wavelengths because of the strong dependence of Rayleigh scattering on wavelength. With longer wavelengths, losses increase because of the intrinsic infrared absorption of the material. Losses of a fraction of a dB/km in solid core PCF have been reported in [7]. The magnitude of dispersion changes with wavelength, passing through zero at 1.3 μm in conventional fiber [4]. Being an important parameter in optical fiber development, the dispersion is naturally also of relevance for PCF technology. Experiments done over the last few years show that PCFs can be designed to use as dispersion compensating fiber (DCF) [5]-[6]. It is possible to shift the zero dispersion wavelengths by changing the geometrical parameters of holey fibers. Group velocity dispersion (GVD) and modal birefringence of PCFs have been discussed using full vector analysis method [7]-[8]. Analysis methods for numerical modeling of photonic crystal fibers have been reviewed in detail, and through the full vector finite element method (FEM), the fundamental characteristics of PCF, e.g., modal birefringence, confinement loss, chromatic dispersion etc have been investigated. Numerical results show very high group birefringence of the order of $10^{-2}$ and phase birefringence of the order of $10^{-3}$ [9]. PCFs have been shown experimentally to have a number of very interesting features, such as a wide single mode wavelength range, large effective mode area, and anomalous dispersion at visible and near infrared wavelengths. As many useful photonic crystal devices have been designed around the PCF concept, it is particularly important to develop a model that is capable of accounting for propagation mechanisms in PCFs. Imaginary distance algorithm and the full vectorial finite element based

3

beam propagation method (IDVFEBPM) have been successfully applied to the modal solutions, both linear and nonlinear, of PCFs [10]. Recently it has been shown that highly birefringence PCFs have the potential to achieve wideband Single-Polarization Single – Mode (SPSM) photonic crystal fibers [11]. Influence of varying PCF parameters on the properties of SPSM operation is also discussed at length. For a number of applications it is essential to design PCFs that offer simultaneously high birefringence, low losses and zero chromatic dispersion at a wide wavelength window. Such a novel PCF having these features has been proposed in [12]. The design features as suggested in this work involve varying geometry in the structure of the proposed PCF. Dispersion and confinement loss properties of PCF with hybrid cladding have been highlighted, and tremendous improvement on these properties has been focused in [13].

## 1.3    Motivation

Numerical analysis technique approaches are used for performing modal analysis of PCFs. Of the numerical techniques, the effective index method [4], the plane wave expansion method [8], the full vectorial finite element based beam propagation method [10], a boundary element method [15], a finite difference approach [16] etc. have been used. This is to mention that most of the numerical analyses are carried out to find the modal solutions of unstressed PCFs. However, the effect of uniform external stress on the propagation properties of PCF has not yet been reported upon. Noteworthy, in order to determine the propagation properties of PCFs considering external stress effects, it is necessary to solve the full vectorial wave equations. Thus, the effects of external stress on birefringence, group velocity dispersion and polarization mode dispersion etc. of PCF are still an area of further study. This unexplored area has motivated us to carry out this research work. In our work, birefringence due to the geometrical anisotropy and the stress induced birefringence are determined for solid core PCFs considering effects of external stress. We have calculated the phase modal birefringence, group birefringence, beat length, group velocity dispersion and polarization mode dispersion of the PCFs considering external uniform stress on the PCF and shown them graphically.

## 1.4    Objectives

On successful completion of this thesis work it is intended to achieve the following objectives:

♦       To carry out the analysis of the effects of thermal and external stress on the propagation properties of photonic crystal fibers.

♦       To incorporate the effects of stress due to the variation of thermal expansion coefficients with the external stress from all sides.

♦       To evaluate the modal birefringence, group birefringence, modal confinement, effective mode area, group velocity dispersion, polarization mode dispersion etc. considering the above system imperfection.

♦       To investigate the influence of core size and the number of the layers of air hole rings on all these properties.

♦       To evaluate the effect of wavelength dependence of the propagation properties of PCFs under external stress..

To achieve these objectives, the finite element method (FEM) as discussed in [14]-[16] is employed using the COMSOL multiphysics (version 3.2a) software to perform the accurate modal analysis of the solid core PCF under external stress. The effective index, phase modal birefringence, group birefringence, beat length, effective mode area, group velocity dispersion, polarization mode dispersion etc. have been calculated and presented graphically in this paper. In the process, the influence of the geometrical structure (core size, air hole diameter, number of the layer of air hole rings etc.) on the leading properties of the PCF has also been discussed in the work.

## 1.5    Organization of the thesis

**Chapter 1** introduces the thesis topic. Here, an overview of the emergence of the photonic crystal fiber has been described. Thereafter, a review of a good number of literatures has been made on the related fields studied so far. This chapter also contains the motivation that drives us for studying PCF and doing this thesis work. The objectives of the thesis work are also set in this chapter.

**Chapter 2** furnishes a bit detail discussion on the photonic crystal fiber (PCF). At the outset, a brief understanding about the structure and different types of PCFs has been developed. Thereafter, mechanism of light guidance in PCF has been discussed. This chapter also presents some theoretical aspects of salient propagation properties, like, birefringence, beat length, group birefringence, polarization mode dispersion, group velocity dispersion etc.of optical fibers. .

**Chapter 3** addresses the stress analysis of optical fiber by using Finite Element Method (FEM) and the theory underneath. This chapter introduces a brief tutorial over FEM; it is the idea of using subdomain basis functions that makes it possible to solve complicated boundary value problems. FEM is often characterized as the computer aided analysis method widely used in the majority of engineering fields like electromagnetics, structural analysis, vibration, heat transfer and fluid mechanics. This chapter furnishes the basic steps to be followed for carrying out modal solutions of the PCF considering external stress effects.

**Chapter 4** presents the discussion and graphical presentation of the numerical results obtained through the study and analysis of the propagation properties of PCF considering external stress effects. Modal analyses of solid core PCF under external stress effects has been presented in this chapter.

**Chapter 5** draws a conclusion of this work. This chapter puts forward suggestions for future scopes of works related to this thesis. Research should be continued to find PCFs of different geometry for its versatile use in the fields of communication engineering and optical physics.

# CHAPTER 2

# Introduction to Photonic Crystal Fibers

## 2.1    Background

It is almost always the fact that inventions are the result of a number of different internal and external influences and ideas. The emergence of photonic crystal fiber (PCF) is not an exception to this fact. The invention of photonic crystal fiber dates back to 1991 when Phillip. St. john Russel, for the first time coined the term " Photonic Crystal Fiber" in an unpublished work of his (P. Russel stated in 2003) [1]-[3]. During his Ph.D work at Oxford in 1976, he became interested in borrowing concepts and intuitive tools from other fields, especially the dynamical theory of x-ray diffraction and Floquet-Bloch theory for waves in periodic media [3]. This naturally led to thinking in terms of electromagnetic band-structure. Bloch waves and the curious effects that appear when group and phase velocity point in different directions or when the group velocity is independent of the direction of the incident wave vector. This made P. St. J. Russel very receptive to the suggestions by Eli Yablonovithch and Sajeev John in 1987 that a full electromagnetic band gap might be created by periodically structuring a high refractive index material to produce a photonic band gap crystal. Their main interest lay in creating an absence of photonic states in three dimensions, some thing that Yablonovitch went on to demonstrate experimentally at microwave frequencies. P. Russel quickly realized that one might be able to achieve low loss guidance of light in a hollow fiber core. The challenge would be to increase the scattering sufficiently so that, over a range of axial wave vectors propagation is closed off for all radial and azimuthal directions in the transverse plane - in other words, a two dimensional photonic band gap (PBG) appears.

In general, such fibers have a cross-section (normally uniform along the fiber length) micro structured from two or more materials, most commonly arranged periodically over much of the cross-section, usually as a cladding surrounding a core where light is confined. For example, the fibers first demonstrated by Philip Russell consisted of a hexagonal lattice of air holes in a silica fiber; with a solid core (1996) or hollow core (1998) at the centre where light is guided. Other

arrangements include concentric rings of two or more materials, first proposed as Brags fibers by Yeh and Yariv (1978), a variant of which was recently fabricated by Temelkuran et.al. (2002).

## 2.2 Modes of operation

According to the confinement mechanism, PCFs can be divided into two modes of operation, namely index guiding principle and photonic band gap principle. A solid core PCF, or a core with a higher average index than the microstructured cladding, can operate on the same index guiding principle as the same optical fiber. However, they can have a much higher effective-index contrast between core and cladding. Therefore, solid core PCF can have much stronger confinement for applications in nonlinear optical devices, polarization maintaining fibers. On the other hand, in photonic band gap fiber, light is confined by a photonic band gap created by the microstructured cladding such a band gap, properly designed, can confine light in a lower effective index core and even a hollow (air) core [5]-[6] . Band gap fibers with hollow cores can potentially circumvent limits imposed by available materials, for example, to create fiber that guide light in wavelength for which transparent material are not available. Another potential advantage of a hollow core is that one can dynamically introduce materials into the core, such as a gas that is to be analyzed for the presence of some substance.

## 2.3 Photonic crystals – the origin of PCF

The idea of photonic crystal originated back in 1987 when it was shown that in periodic arrangements of ideally lossless dielectrics, the propagation of light can be totally suppressed at certain wavelengths, regardless of propagation direction and polarization. This inhibition does not result from absorption but rather from the periodicity of the arrangement and is quite fundamental in the frequency range where no propagation is possible (the so called photonic band gap). Such periodic arrangements of dielectrics have been called photonic crystals or photonic band gap materials [5]. Photonic crystals are today used as a general term describing periodic structures both in one, two, and three dimensions. While structures with a periodicity in one dimension (1D) have been known and exploited for decades, e.g., finding use in high reflection mirrors and fiber Bragg gratings , their two and three dimensional (2D and 3D) counterparts have only been explored since the publications of the original ideas of Yablonovitch

and John in 1987 [6]. Photonic crystals are attractive optical materials for controlling and manipulating the flow of light.

## 2.4  One dimensional photonic crystal : Bragg mirrors

The simplest device using the principles of photonic crystals is the one dimensional photonic crystal, well known as Bragg mirror or the multilayer reflector. It consists of a periodic stack of two alternating dielectric layers. Light propagating in a direction normal to the layers undergoes successive reflection and transmission at each interface between adjacent layers. With an appropriate choice of layer thickness and refractive indices, waves reflected from each interface are in phase, whereas waves transmitted are out of phase. In that case, the transmitted wave components cancel each other out, and only the interference of the reflected components constructive: the light is totally reflected. This works for a range of wavelengths. Bragg mirrors have been in use for decades, but it is only recently that they have come to be regarded as a special case of photonic crystal [4].

## 2.5  Photonic crystals in two and three dimensions

Photonic crystals with two dimensional periodic arrangement are usually either made of paralleled dielectric or metallic rods in air, or through drilling or etching holes in a dielectric material. In the field of integrated optics, holes of a fraction of a micrometer for integrated photonic circuits have been successfully demonstrated experimentally. The two dimensional photonic crystals may be utilized to reflect light in the out-of-plane case, i.e., for waves propagating at an oblique angle to the holes/rods of the photonic crystal [5].

Photonic crystals with three dimensional periodicity is a bit trickier to achieve. However, it can be made by drilling an array of holes at three different angles into a dielectric material as suggested by Yablovitch [5]. However, the scalability discussed in one dimensional periodic case is valid for two dimensional and three dimensional structures all well. Many experimental studies of 2D and 3D periodic structure have, therefore been performed at microwave frequencies. This allowed in 1991 Yablonovitch to demonstrate the first structure exhibiting a full three dimensional photonic band gap [5]. Nevertheless, the 3D photonic crystal is still far

from commercialization but offer additional features possibly leading to new device concepts, e.g., optical computers [27] when some technological aspects such as manufacturability and principal difficulties such as disorder are under control.

## 2.6    Guiding light in photonic crystals

In an infinite photonic crystal with band gap structure for frequencies within a total photonic band gap, no propagation is allowed. Localized defect states for isolated frequencies within the band gap can emerge (similar to bond states associated with defects in semiconductor) if a defect is introduced in infinite lattice. For three dimensional photonic crystal lattices, this can be a single point defect: in that case light emitted from within the defect will remain confined in the vicinity of the defect. Another way of looking at defect states is to consider the photonic crystal to be a perfect mirror in a certain frequency range. If one drills a hole all the way through the photonic crystal, light injected in the hole will be reflected at the borders of the hole and will propagate within it similar way to that of light propagation in an optical fiber [5].

Given that photonic crystals can have a high reflection coefficient even with a relatively small number of periods, the width of the photonic crystal around the defect can be reduced to a few layers: we can hence imagine optical fibers consisting of a micrometric core surrounded by a photonic crystal cladding only a few times wider than the core. The resulting optical fiber is celled a "Photonic Crystal Fiber" and has an important difference from conventional optical fibers. As we know in case of conventional optical fiber, the core in which light is guided has to be of higher refractive index than the cladding. Using a photonic band gap material for the cladding, the reflection at some frequency is guaranteed regardless of the refractive index of the material inside the defects. A defect in a photonic crystal can hence confine and guide light in low refractive index media, such as a gas (may be air) or vacuum. This opens up possibilities ever dreamt before. An optical fiber guiding light in a vacuum would have absorption losses and non-liner effects reduced by orders of magnitude compared with solid core fibers, paving the way for high power light guidance applications; material dispersion would become negligible, giving rise to completely new forms of dispersion management; guiding highly confined light in gas or liquids would enable the production of new types of non-liner fibers as well as a whole new family of fiber sensors, even guidance of atoms, molecules or cells through hollow core optical fibers would become possible [5]

10

## 2.7 Types of photonic crystal fiber

The general terms holey fiber and microstructured optical fiber (MOF) refer to any kind of fiber with a set of inclusions running along the fiber axis, whereas the term photonic crystal fiber is generally used to refer to MOFs in which guidance results from a photonic band gap effect. Again, however, some authors also use the term photonic crystal fiber (PCF) for referring to MOFs in which the inclusions form a subset of a periodic array, but in which guidance may or may not result from photonic band gap effects [5] - [6]. Thus specific categories of PCF include photonic band gap fiber-PCFs that confine light by band gap effects; holely fiber-PCFs that use air holes in their cross sections; hole assisted fiber-PCFs guiding light by a conventional higher index core modified by the presence of air holes and Bragg fiber-photonic band gap fiber formed by concentric rings of multilayer film [27]. However, brief description of the two main categories of PCF, viz, the photonic band gap fiber and the holey fiber would be furnished in the following sub sections.

## 2.7.1 Photonic bandgap fiber (PBGF)

Light guidance in hollow core MOFs can only be achieved by using the photonic band gap effect. Hollow core MOFs are hence necessarily photonic crystal fiber. We must consider a two dimensional photonic crystal with a one dimensional defect. For a silica matrix with a triangular lattice of circular air holes, there is no complete photonic bandgap in the transverse propagation plane due to the low contrast in index between the two regions. Nevertheless, for propagation constant, $\beta \neq 0$ bandgap appears allowing the use of silica hollow core MOFs. Inserting a defect in the middle of the photonic crystal structure will make possible the existence of a propagating mode in the perturbed crystal. If propagation constant, $\beta$ of this mode coincides with a bandgap in the transverse plane then the mode will be confined in the locality of the defect, which constitutes the hollow core of the MOF. Light guidance being possible solely within a photonic bandgap, the wavelength range in which these fibers guide light is very narrow (only a few tens of nanometers) for guidance in the infrared or the visible spectrum. Furthermore, the accuracy of the periodicity of the lattice required to obtain a clear bandgap effect makes the fabrication of these fibers challenging. In 1999 the first hollow core PCF was reported and the best hollow-

core transmission losses now stand at 1.1 dB/km at 1550 nm [18]. The Fig. 2.1 shows the schematic diagram of the cross section of a hollow core PCF..
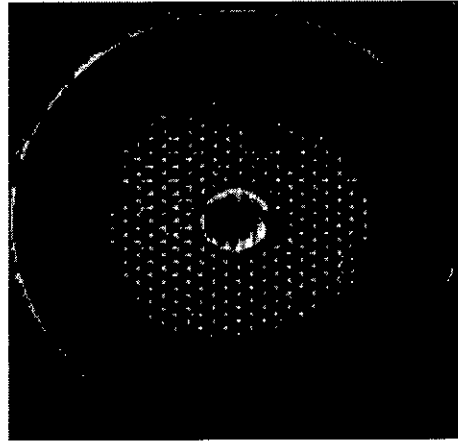


Fig. 2.1 : Schematic diagram of the cross section of a hollow core PCF (reference: www.bath.ac.uk/bandgap)

## 2.7.2 Solid core photonic crystal fiber

Photonic crystal fibers with a solid core or a core with a structured cladding can operate on the same index-guiding principle as conventional optical fiber. However, they can have a much higher effective index contrast between core and cladding, and therefore, can have much stronger confinement for applications in nonlinear optical devices [19]. In the holey fiber, the core is a deliberate defect region, where there is a missing air hole in the centre. In such holey fiber, the core index is greater than the average index of the cladding because of the presence of the air holes, and the fiber can guide light by total internal reflection as a standard fiber does. That is the guided light has an effective index, $n_{eff}$, which satisfies the condition.

$$n_{c0} > n_{eff} = \beta/k_0 \qquad (2.1)$$

where, $\beta$ is the propagation constant along the fiber axis, $k_0$ is the free space wave number, $n_{c0}$ is the core index. The solid core PCF is relatively easier to fabricate than PBG fiber. The only true difference with bandgap guidance using other PBG fiber is that the bandgap between $\beta$ max

12

and $\beta = \alpha$ always exists, regardless of frequency or the exact structure of the cladding so that guidance relying on this band gap so much easier to achieve [5]. The Fig. 2.2 shows the schematic diagram of the cross section of a solid core PCF.
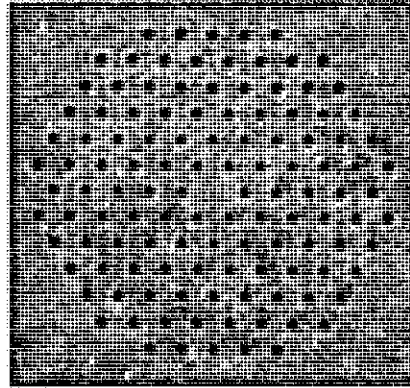


Fig. 2.2 : Schematic diagram of the cross section of a solid core PCF (reference: www.pcfiber.com)

## 2.8    Salient properties of PCF

Study and analysis on solid core PCF showed that these fibers possess unique properties of their own, unachievable by conventional optical fibers. PCFs have ability to be single mode over an infinite range of wavelengths. The next prominent feature is the light confinement. Because of the large refractive index contrast (1.46:1) [3], modes are very well confined in the core, even when the wave length to core size ratio is not small. Good confinement in small cores enables higher power densities and hence accentuated non-liner properties [5].

The large available parameter space of solid core MOFs makes the wave length dispersion, which can have strong effect due to the high index contrast, highly configurable. Almost any dispersion curve seems accessible to MOFs with the correct design. The combination of endlessly single mode guidance and adjustable dispersion has led to solid core, single mode MOFs with anomalous dispersion, to single mode fibers with a zero dispersion wavelength shifted down to the visible as well as to single mode fibers with ultra-flat normal or anomalous dispersion over a large wave length range [4]-[5].

## 2.9  Single mode single polarization fibers

Single polarization single mode (SPSM) fibers that guide only one polarization mode were first proposed in the 1980s [11]. These fibers guide one polarization of the fundamental mode only, while the other orthogonal polarization mode is eliminated. A very large refractive index difference between the core and the cladding region is required to make SPSM fibers. This may be the reason why it is difficult to realize wide band SPSM operation in conventional fibers. We know that PCFs are usually made from a single material, e.g. pure silica, with an array of air holes in the cladding that run along the length of the fiber. By having different air hole diameters along the two orthogonal axes or changing the air hole arrangement in the cladding region, PCFs with modal birefringence can be easily achieved because the index contrast is higher than that in conventional fibers [11]. In solid-core PCF with the symmetries of the lattices of holes that are generally used in practice (mostly six or four fold symmetry), this results in the fundamental mode being doubly degenerate, as in conventional optical fibers. If the core is now extended to two adjacent missing holes, or if the symmetry around the core is reduced to two-fold symmetry (e.g. through changing the sizes of two diametrically opposed holes, or with elliptical holes), the degeneracy is lifted and the fiber becomes birefringent, and the PCF becomes polarization maintaining fibers. SPSM fibers can be achieved in the same way. These polarization maintaining fibers are highly useful as sensing devices and in communication systems [11], [19]-[20]

## 2.10  Applications of PCF

One particularly attractive feature of PCF structures is that they are highly uniform over very long distances. This means that light launched in at one end has time to sort itself out into a single mode, permitting highly reproducible detection of very small effects. Essentially unwanted cladding modes are efficiently filtered out before they can interfere with the measurements. This is in sharp contrast to most other kinds of photonic crystals, where taking reliable optical measurements is a challenging and painstaking process. As a result, new PCF structure and PCF-based applications can rapidly be developed, perhaps the most celebrated being the report in 2000 of super continuum generation from un-amplified Ti: sapphire fs laser pulses in a PCF with a core small enough to give zero dispersion at 800 nm wave length. [5].

14

Thus PCFs are of great interest for optical communication in new wavelength regions and for new optical devices. Hollow core PCF has many fascinating applications including gas-Raman cell for high efficiency, low threshold color-conversion of laser light, and laser-tweezers propulsion and guidance of small particles along a curved path. Another relatively unexplored area is optical sensing, with huge opportunities spanning many fields including environmental detection, bio-medical sensing and structural monitoring [4]-[6].

It is worth mentioning here that not only can the fiber be stretched locally to reduce its cross-sectional area, but the micro structure can itself be radically altered. Components (Couplers, filters, transitions etc) made in this way have one great advantage over equipment devices made in conventional fiber: being formed by permanent changes in structure they are highly stable with temperature and over time. It is clear that many exciting developments are emerging and will emerge based on PCF in its many forms with applications spanning many disparate fields of science [I]-[3].

## 2.11  Stress optic effects of PCF

The conventional optical fiber consists of the core and the cladding made of two different materials having different coefficients of thermal expansion. When the fiber is cooled down from a higher temperature (melted condition) to the ambient temperature during the manufacturing process, due to the different coefficients of thermal expansion, mechanical stress is introduced in the fiber with greater value at the core-cladding interface region. The mechanical stress on the optical fiber can also originate from a variety of other sources. One source that is very difficult to control is the diurnal (day/night) and seasonal heating and cooling of the fiber. Although much fiber is laid down in the ground and often within conduits, it is still subject to temperature variations and corresponding mechanical stress. Another source of mechanical stress can originate from nearby sources of vibration. For example, much fiber is deployed alongside railroad tracks because of the ease of right-of-way and construction. However, vibration from passing trains can contribute to stress on the optical fiber.

We know that PCF is made from the same material where the refractive index contrast between the core and the cladding region is achieved by creating periodic arrays of rings of air holes that run along the length of the fiber. In a band gap PCF, there is an air hole deliberately created in the centre of the fiber. On the other hand, in a solid core PCF, there is deliberate missing of an

15

air hole in the centre of the PCF. Here also thermal stress will be introduced because of the difference in thermal expansion coefficients of the PCF material and air. The PCF will be subject to other sources of mechanical stress as it is in the case of conventional PCF. Thus it is evident that in PCFs under thermal and external stress, the refractive index of the material changes due to the photonic effect. Effect of lateral stress including thermal stress on the properties of PCF has been studied in [19]-[20]. Therefore, in this work, effect of uniform external stress including thermal stress on the properties of a solid core PCF has been addressed. The finite element method (FEM) [14] has been used to carryout modal analysis of the light wave propagating in the PCF. COMSOL Multiphysics, version 3.2a [31] and MATLAB, version 7.0 [32] have been used as software tools throughout the research work. First, stress analysis is done to find the new anisotropic refractive index of the fiber material under the stress effect (both thermal and external) associated with the PCF. Thereafter, optical analysis has been done to determine other salient optical properties of the PCF.

## 2.12   Propagation properties of PCF

Before going into detail discussions on the properties of PCF, let us highlight a few definitions of related terms.

**Effective index**

Effective index is a number quantifying the phase delay per unit length in a waveguide relative to the phase delay in vacuum. In a usual single-mode fiber, the guided propagation mode extends significantly beyond the region of the fiber core, and the effective refractive index is found to have a value somewhat between the refractive indices of core and cladding. In a multimode fiber, higher-order modes extend more into the cladding, and have smaller effective indices. But effective index is not a kind of weighted average of the local refractive index. The effective index, $n_{eff}$ can be defined as the propagation constant of some fiber mode is $n_{eff}$ times the vacuum wave number. So that definition targets the phase change per unit length along the fiber axis, not the intensity distribution. In case of a step-index multimode fiber with high numerical aperture (NA), all fiber modes propagate essentially only in the core; so that from this one might expect the effective index of all modes to closely match the core index. But this is not the case: higher-order modes still have significantly lower effective indices. They experience a smaller phase

shift per unit length, even though they propagate in the same material. Essentially it is the fact that higher-order modes contain more pronounced plane wave components (spatial Fourier components) with a larger angular offset from the fiber axis. So it is here in some sense a matter of different propagation directions, not of different materials. Of course, both effects are relevant in fibers with lower NA. Modes with stronger off-axis field components do not experience a larger rather than a smaller phase shift per unit length, given that they somehow have to travel a larger distance. When the k vector has some angle to the fiber axis, its projection to the fiber axis becomes smaller, reducing the phase changes in that direction.

**Group index**

A "group velocity refractive index", usually called the *group index* is defined as

$$n_g = \frac{c}{v_g} \tag{2.2}$$

where $v_g$ is the group velocity. This value should not be confused with $n$, which is always defined with respect to the phase velocity. The group index can be written in terms of the wavelength dependence of the refractive index as

$$n_g = n - \lambda \frac{dn}{d\lambda} \tag{2.3}$$

where $\lambda$ is the operating wavelength.

**Group velocity dispersion (GVD)**

In optics, dispersion is the phenomenon in which the phase velocity of a wave depends on its frequency. Media having such a property are termed as dispersive media. Another consequence of dispersion manifests itself as a temporal effect. The formula $v = c/n$ calculates the phase velocity of a wave; this is the velocity at which the phase of any one frequency component of the wave propagates. This is not the same as the group velocity of the wave, which is the rate that changes in amplitude (known as the envelope of the wave) will propagate. The group velocity, $v_g$ is related to the phase velocity by, for a homogeneous medium, (here, $\lambda$ is the operating wavelength in vacuum):

$$v_g = c(n - \lambda \frac{dn}{d\lambda}) \tag{2.4}$$

The group velocity, $v_g$ is often thought of as the velocity at which energy or information is conveyed along the wave. In most cases this is true, and the group velocity can be thought of as the signal velocity of the waveform. In some unusual circumstances, where the wavelength of the light is close to an absorption resonance of the medium, it is possible for the group velocity to exceed the speed of light ($v_g > c$), leading to the conclusion that superluminal (faster than light) communication is possible. In practice, in such situations the distortion and absorption of the wave is such that the value of the group velocity essentially becomes meaningless, and does not represent the true signal velocity of the wave, which stays less than $c$ [30]

The group velocity itself is usually a function of the wave's frequency. This results in group velocity dispersion (GVD), which causes a short pulse of light to spread in time as a result of different frequency components of the pulse traveling at different velocities. The chromatic dispersion $D$ of a PCF is calculated from the effective index of the fundamental mode, $n_{eff}$ versus the wavelength as under

$$D = -\frac{\lambda}{c} \frac{d^2 n_{eff}}{d\lambda^2} \tag{2.5}$$

where, $c$ is the velocity of light in a vacuum, $n_{eff}$ is the refractive index of the PCF and $\lambda$ is the operating wavelength.

If $D$ is less than zero, the medium is said to have *positive dispersion*. If $D$ is greater than zero, the medium has *negative dispersion*. If a light pulse is propagated through a normally dispersive medium, the result is the higher frequency components travel slower than the lower frequency components. The pulse therefore becomes positively chirped, or up-chirped, increasing in frequency with time. Conversely, if a pulse travels through an anomalously dispersive medium, high frequency components travel faster than the lower ones, and the pulse becomes negatively chirped, or down-chirped, decreasing in frequency with time.

The result of GVD, whether negative or positive, is ultimately temporal spreading of the pulse. This makes dispersion management extremely important in optical communications systems based on optical fiber, since if dispersion is too high, a group of pulses representing a bit-stream will spread in time and merge together, rendering the bit-stream unintelligible. This limits the

18

length of fiber that a signal can be sent down without regeneration. One possible answer to this problem is to send signals down the optical fiber at a wavelength where the GVD is zero (e.g. around ~1.3-1.5 µm in silica fibers) [22]. So pulses at this wavelength suffer minimal spreading from dispersion—in practice, however, this approach causes more problems than it solves because zero GVD unacceptably amplifies other nonlinear effects (such as four wave mixing). Another possible option is to use soliton pulses in the regime of anomalous dispersion, a form of optical pulse which uses a nonlinear optical effect to self-maintain its shape. However, solitons have the practical problem that they require a certain power level to be maintained in the pulse for the nonlinear effect to be of the correct strength [29]. Instead, the solution that is currently used in practice is to perform dispersion compensation, typically by matching the fiber with another fiber of opposite-sign dispersion so that the dispersion effects cancel; such compensation is ultimately limited by nonlinear effects such as self-phase modulation, which interact with dispersion to make it very difficult to undo. PCFs find its tremendous usefulness in this regard [1]-[11].

**Group Birefringence**

The group birefringence can be defined with the mathematical expression as

$$B_g = B - \lambda \frac{dB}{d\lambda} \tag{2.6}$$

where, $B$ is the phase index birefringence, defined as

$$B = \left| n_{eff}^x - n_{eff}^y \right| \tag{2.7}$$

where, $n_{eff}^x$ and $n_{eff}^y$ are the effective refractive indices of the fundamental $x$ and $y$ polarization modes, respectively [9]

**Beat Length**

Highly birefringence fibers are widely used in optical sensors, precious optical instruments, and optical communication systems. Birefringence is defined as a difference between effective

refractive indices of two fundamental polarization modes ($HE_{11}^x$ and $HE_{11}^y$) [12] and can be written as

$$B = \left| n_x - n_y \right| \qquad (2.8)$$

where, $n_x$ and $n_y$ are the effective refractive indices of each fundamental mode. If light is injected into the fiber so that both modes are excited, then one will be delayed in phase relative to the other as they propagate. When this phase difference is an integral multiple of $2\pi$, the two modes will beat at this point and the input polarization state will be reproduced. The length over which this beating occurs is the characteristic length or fiber beat length (measured in meter) [21], and mathematically expressed as

$$L_B = \frac{\lambda}{B} \qquad (2.9)$$

where, $B$ is the phase modal birefringence and $\lambda$ is the optical wave length.

**Effective Mode Area**

The effective mode area of the PCF, $A_{eff}$ is defined as

$$A_{eff} = \frac{\iint_S \left\{ \left| E_t \right|^2 dxdy \right\}^2}{\iint_S \left| E_t \right|^4 dxdy}, \qquad (2.10)$$

where, $E_t$ the transverse electric field vector and $s$ denotes the whole fiber cross section [8]. It is learnt that increasing the air hole size, the mode becomes more confined in an unstressed PCF, and thus the effective mode area is reduced. On the other hand, the effective area is almost independent of the number of air hole rings [8].

## 2.13 Polarization Mode Dispersion

Polarization mode dispersion (PMD) arises when two orthogonal states of polarization propagate at different velocities in optical fibers. PMD is one of the fundamental limitations on high speed, high bit rate communication in fiber systems because it distorts the shape of light pulses, and in particular induces pulse spreading. Hence much effort has gone into reducing PMD in optical fibers. PMD arises because of uncontrolled stresses or anisotropies induced in the fiber during

20

the manufacturing process and during deployment. These cause unwanted birefringence, and hence PMD. This residual birefringence changes randomly along the fiber, resulting in random mode coupling as the light propagates along the fiber. Because of this statistical process, the effects of PMD such as pulse spreading increases as the square root of the propagation distance. This statistical process makes it extremely difficult to correct the effects of PMD after the light has propagated through a long length of fiber. For this reason one rather tries to reduce the PMD of the fiber itself.

When light travels down a single mode fiber toward the receiver, it has two polarization modes that follow the path of two axes. They move toward the receiver at right angles to each other. When the core of the fiber that bounds the light is asymmetrical, the light traveling along one polarization axis moves slower or faster than the light polarized along the other axis. This effect can spread the pulse enough to make it overlap with other pulses or change its own shape enough to make it undetectable at the receiver.
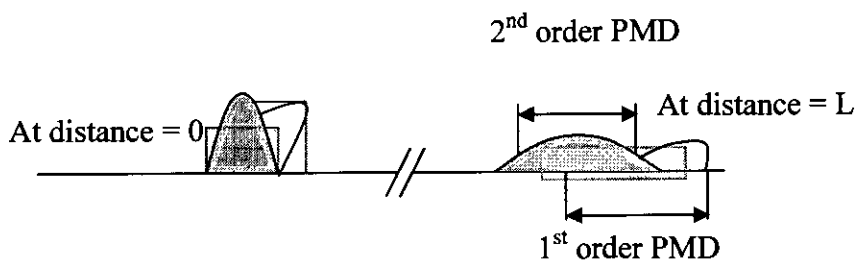


Fig. 2.3: Graphical Representation of the Effect of PMD on an Optical Pulse

In Fig. 2.3, the optical pulse and its constituent photons travel from the source, or transmitter, at distance = 0, along the single-mode optical fiber. At some distance after PMD has affected the pulse, the polarized energy is separated by some time. This time is known as differential group delay (DGD). DGD is the fundamental measure of PMD and is measured in picoseconds ($10^{-12}$ sec). If DGD is severe, the receiver at some distance $L$ cannot accurately decode the optical pulse, and bit errors can result.

**Tolerable PMD**

The tolerable level of system PMD depends on data rate, distance and how much system outage one is willing to tolerate. The average system outage is a function of system PMD for 10, 40 and 80 Gbps systems. As the system PMD limit for a given bit rate is approached, slight increases in

21

PMD will cause significant increases in system outage. International standard guidelines for PMD recommend an outage probability of 6.5 x $10^{-8}$, corresponding to 2 seconds of outage per year attributable to PMD. A goal for a 10 Gbps system would be a cabled optical fiber with ~4 ps of total PMD. This drop to below 1 ps if a 40 or 80 Gbps system is envisioned operating on this fiber in the future.

The PMD requirement on the cabled fiber is dependent on the distance of the route. For example if we have a 100 km link at 10 Gbps, then the cabled fiber should have a LDV below 0.4 ps/sqrt(km) but at 40 Gbps, this same route requires an LDV below 0.1 ps/sqrt(km). For longer distances, the LDV requirements become even more stringent such that at 1000 km, a 10 Gbps system would require a cabled fiber LDV of <0.13 ps/sqrt(km) while a 40 Gbps system would need a value <0.03 ps/sqrt(km).

## 2.14 Relation among Birefringence, PMD and DGD

Birefringence, as discussed in previous section is expressed as

$$B = \left| n_x - n_y \right|$$ (2.11)

where, $n_x$ and $n_y$ are the effective refractive indices of each fundamental mode or double refraction, is the decomposition of a light ray into two rays (the ordinary ray and the extraordinary ray), depending on the polarization of the light.

Polarization mode dispersion (PMD) is a form of modal dispersion where two different polarizations of light in a waveguide, which normally travel at the same speed, travel at different speeds due to random imperfections and asymmetries, causing random spreading of optical pulses. It is the average differential group delay (DGD) one expects to see when measuring an optical fiber. DGD is the time separation or delay between the two principal polarization modes of the transmission link at the receiver. DGD is an instantaneous event and varies randomly with wavelength and time. This means that DGD is a statistical parameter, obeys the laws of probability theory and thus has uncertainty associated with it. PMD is the average value of a distribution of a large number of independent DGD measurements [30]. Phase delay $\beta$ and the

group delay $G_d$ can be used to characterize the corresponding type of birefringence. The phase delay $\beta$ [rad/m] and the phase birefringence $B$ can also be expressed as [21]

$$\beta = \beta_x - \beta_y \tag{2.12}$$

where, $\beta$ is the phase delay (rad/m), $\beta_x$ and $\beta_y$ are the propagation constants of the two orthogonally polarized modes of propagation. The modal (phase) birefringence, $B$ can be expressed with respect to the phase delay as

$$B = \frac{\beta}{2\pi / \lambda} \tag{2.13}$$

Now, Beat length is expressed as

$$L_B = \frac{\lambda}{B} \tag{2.14}$$

where, $\lambda$ denotes the optical wavelength.

The group delay $G_d$ is defined as the frequency derivative of the phase birefringence and is given by

$$G_d = \left| \frac{\partial B}{\partial \omega} \right| = \left| B - \lambda \frac{\partial B}{\partial \lambda} \right| = B_g \tag{2.15}$$

where, $B$ denotes phase birefringence and $\omega$ is the optical frequency.

Again, the group modal birefringence $B_g$ is directly proportional to polarization mode dispersion (PMD), and is measured in terms of $B_g$, by the following working equation [20]

$$\tau_g = \frac{B_g}{c} \tag{2.16}$$

where, c is the velocity of light in vacuum and $\tau_g$ is the PMD.

# CHAPTER 3

# Stress Analysis of Photonic Crystal Fibers

## 3.1 Energy Conservation Principle

The energy principle states that the total potential energy should be a minimum when thermal stress and/or an external force is applied to the body. In other words, the strain distribution that is actually generated among all possible strain profiles is the distribution that makes the potential energy a minimum. The total potential energy of the body is given by [14]

$$\Pi = (\text{internal work}) - (\text{external work}) = U - V, \tag{3.1}$$

where, U and V denote strain energy and work done by the external force, respectively. Strain energy U is work generated during the process of releasing strain; i.e., U is a summation of {local force generated under certain strain condition}×{displacement by the force}. Since potential energy decreases by the amount of work done by the external force, V has a minus sign in (3.1).

Stress analysis based on the energy principle is called the energy method. The finite element method (FEM) based calculation procedure is as follows [14]:

- Express the potential energy $\Pi$ in terms of the displacement by strain and an external force.
- Approximate the displacement and external force in or toward each element by analytical functions using values at nodal points.
- Apply the energy principle to $\Pi$; i.e., partially differentiate $\Pi$ with respect to the displacement and obtain an equilibrium equation (linear simultaneous equations).
- Solve the simultaneous equations and determine the displacement at each nodal point.
- The strain and stress in each element are calculated by using the displacement at the nodes surrounding the element.

## 3.2 Stresses and strain in terms of displacements

The optical fiber is always very long in one dimension (along z-axis direction) and very limited in the other two transverse dimensions. In such a case, strain in the body along z-axis $\varepsilon_z$ is considered to be negligible, except at both ends. Thus, we can assume

$$\varepsilon_z = 0. \tag{3.2}$$

Stress analysis based on this assumption is called a "plane strain problem". The relationship between displacement and strain is given by [14]

$$\varepsilon_x = \frac{\partial u}{\partial x}, \tag{3.3}$$

$$\varepsilon_y = \frac{\partial v}{\partial y}, \tag{3.4}$$

$$\text{and} \quad \gamma_{xy} = \frac{\partial v}{\partial x} + \frac{\partial u}{\partial y}. \tag{3.5}$$

Here, u and v are displacements along the x and y axis directions, respectively, and are in general approximated as functions of x and y. $\varepsilon_x$, $\varepsilon_y$, and $\varepsilon_z$ are spatial variations of the principal strains along the x-, y-, and z-axis directions, respectively, and $\gamma_{xy}$ is the shear strain in the x-y plane. For linear elastic material, the stress-strain relations come from generalized Hooke's law. For isotropic materials, the two material properties are the Young's Modulus (or modulus of elasticity) and the Poisson's ratio. Another type of deformation occurs in the body which is due to the temperature change. For isotropic material change in temperature results in a uniform strain, which depends on the coefficient of linear expansion $\alpha$ of the material. $\alpha$, which represents the change in length per unit temperature change, is always assumed to be constant within the range of variation of the temperature. Also, this strain does not cause any stresses when the body is free of deform. The temperature strain is usually considered as an initial strain. Therefore, combining the Hooke's law and the temperature strain, the relationship between the stress and the strain is generally expressed as [14]

$$\varepsilon_x = \frac{1}{E}[\sigma_x - \mu(\sigma_y + \sigma_z)] + \alpha \Delta T, \tag{3.6}$$

$$\varepsilon_y = \frac{1}{E}[\sigma_y - \mu(\sigma_z + \sigma_x)] + \alpha \Delta T, \tag{3.7}$$

$$\varepsilon_z = \frac{1}{E}[\sigma_z - \mu(\sigma_x + \sigma_y)] + \alpha \Delta T, \tag{3.8}$$

$$\gamma_{xy} = \frac{\tau_{xy}}{G} = \frac{2(1+\mu)}{E}\tau_{xy}, \tag{3.9}$$

Where $\sigma_x$, $\sigma_y$, and $\sigma_z$ are spatial variations of the principal stresses along the x-, y-, and z-axis directions, respectively, $\tau_{xy}$ is the shear stress in the x-y plane, G, $\alpha$, and $\Delta T$ denote the shear modulus (or modulus of rigidity), the thermal expansion coefficient, and the temperature change (negative for cooling), respectively, E and $\mu$ are the Young's Modulus and he Poisson's ratio, respectively. Considering the problem to be a 'plane strain problem', we can get the following relations between the stress and the strain

$$\sigma_x = \frac{E}{(1+\mu)(1-2\mu)}\left[(1-\mu)\varepsilon_x + \mu\varepsilon_y\right] - \frac{\alpha E \Delta T}{(1-2\mu)}, \qquad (3.10)$$

$$\sigma_y = \frac{E}{(1+\mu)(1-2\mu)}\left[\mu\varepsilon_x + (1-\mu)\varepsilon_y\right] - \frac{\alpha E \Delta T}{(1-2\mu)}, \qquad (3.11)$$

$$\sigma_z = \mu(\sigma_x + \sigma_y) - \alpha E \Delta T. \qquad (3.12)$$

For "plane strain problem", the components of stress and strain are expressed in vector form as

$$\{\sigma\} = \begin{bmatrix} \sigma_x \\ \sigma_y \\ \tau_{xy} \end{bmatrix}, \qquad (3.13)$$

$$\{\varepsilon\} = \begin{bmatrix} \varepsilon_x \\ \varepsilon_y \\ \gamma_{xy} \end{bmatrix}. \qquad (3.14)$$

Using (3.13)-(3.14), the relationship between the stress and the strain of the "plane strain problem" as defined by (3.9) and (3.10, 3.20, 3.21), can be expressed as

$$\{\sigma\} = [D](\{\varepsilon\} - \{\varepsilon_0\}), \qquad (3.15)$$

where, the 3×1 initial strain vector $\{\varepsilon_0\}$ due to the thermal strain and the 3×3 matrix [D] are given by

$$\{\varepsilon_0\} = (1+\mu)\alpha\,\Delta T \begin{bmatrix} 1 \\ 1 \\ 0 \end{bmatrix}, \qquad (3.16)$$

and $[D] = \dfrac{E}{(1+\mu)(1-2\mu)} \begin{bmatrix} (1-\mu) & \mu & 0 \\ \mu & (1-\mu) & 0 \\ 0 & 0 & (1-2\mu)/2 \end{bmatrix}.$ (3.17)

## 3.3 Finite Element Formulation

Strain energy per unit length is obtained by [14]

$$(\text{strain energy}) = \frac{1}{2} \iint (\text{stress}) \cdot [(\text{strain}) - (\text{initial strain})] \, dx \, dy.$$

Then,

$$U = \frac{1}{2} \iint \{\sigma\}^{T} \big[\{\varepsilon\} - \{\varepsilon_0\}\big] \, dx \, dy,$$ (3.18)

where, $\{\sigma\}^{T}$ represents the transpose of the vector and integration is over the cross-section of the actual structural body under strain and stress. Since strain and stress do not penetrate into the air region, the actual boundary of the body becomes the boundary of the FEM analysis. The displacements $u(x, y)$ and $v(x, y)$ along the x- and y-axis directions in the eth (e = 1—N) element is approximated by the linear function of x and y:

$$u(x, y) = p_0^e + p_1^e x + p_2^e y,$$ (3.19)

$$v(x, y) = q_0^e + q_1^e x + q_2^e y,$$ (3.20)

where, $p_0^e$, $p_1^e$, $p_2^e$ and $q_0^e$, $q_1^e$, $q_2^e$ are expansion coefficients. Assuming the displacements at nodal points i, j, and k in the $e^{th}$ element are given by $(u_i, v_i)$, $(u_j, v_j)$ and $(u_k, v_k)$, respectively, the expansion coefficients p's and q's are obtained by solving the linear equations which can be obtained from (3.19, 3.20) for the nodal displacements corresponding to the 3 nodal points i, j, and k of the $e^{th}$ element. Thus, one can obtain

$$\begin{bmatrix} p_0^e \\ p_1^e \\ p_2^e \end{bmatrix} = \big[ C^e \big] \begin{bmatrix} u_i \\ u_j \\ u_k \end{bmatrix},$$ (3.21)

27

$$\begin{bmatrix} q_0^e \\ q_1^e \\ q_2^e \end{bmatrix} = \begin{bmatrix} C^e \end{bmatrix} \begin{bmatrix} v_i \\ v_j \\ v_k \end{bmatrix},$$

(3.22)

where, $[C^e]$ is given by

$$\begin{bmatrix} C^e \end{bmatrix} = \begin{bmatrix} 1 & x_i & y_i \\ 1 & x_j & y_j \\ 1 & x_k & y_k \end{bmatrix}^{-1},$$

i.e., $\begin{bmatrix} C^e \end{bmatrix} = \dfrac{1}{2s_e} \begin{bmatrix} (x_j y_k - x_k y_j) & (x_k y_i - x_i y_k) & (x_i y_j - x_j y_i) \\ (y_j - y_k) & (y_k - y_i) & (y_i - y_j) \\ (x_k - x_j) & (x_i - x_k) & (x_j - x_i) \end{bmatrix}.$

(3.23)

Here, the coordinates of the nodal points of the triangular element are expressed as $(x_m, y_m)$ $(m = i, j, k)$. Hence, the cross-sectional area $s_e$ of the $e^{th}$ element is given by

$$2s_e = (x_j - x_i)(y_k - y_i) - (x_k - x_i)(y_j - y_i).$$

(3.24)

Now, we find the strain components in the eth element as

$$\varepsilon_x = \frac{\partial u}{\partial x} = p_1^e = \frac{1}{2s_e}\left[(y_j - y_k)u_i + (y_k - y_i)u_j + (y_i - y_j)u_k\right],$$

(3.25)

$$\varepsilon_y = \frac{\partial v}{\partial y} = q_2^e = \frac{1}{2s_e}\left[(x_k - x_j)v_i + (x_i - x_k)v_j + (x_j - x_i)v_k\right],$$

(3.26)

$$\gamma_{xy} = \frac{\partial v}{\partial x} + \frac{\partial u}{\partial y} = q_1^e + p_2^e = \frac{1}{2s_e}\left[(y_j - y_k)v_i + (y_k - y_i)v_j + (y_i - y_j)v_k\right] + \frac{1}{2s_e}\left[(x_k - x_i)u_i + (x_i - x_k)u_j + (x_j - x_i)u_k\right].$$

(3.27)

28

Therefore, we get the strain vector in each element as

$$
\begin{bmatrix} \varepsilon_x \\ \varepsilon_y \\ \gamma_{xy} \end{bmatrix} = \frac{1}{2s_e} \begin{bmatrix} (y_j - y_k) & 0 & (y_k - y_i) & 0 & (y_i - y_j) & 0 \\ 0 & (x_k - x_j) & 0 & (x_i - x_k) & 0 & (x_j - x_i) \\ (x_k - x_j) & (y_j - y_k) & (x_i - x_k) & (y_k - y_i) & (x_j - x_i) & (y_i - y_j) \end{bmatrix} \begin{bmatrix} u_i \\ v_i \\ u_j \\ v_j \\ u_k \\ v_k \end{bmatrix}. \tag{3.28}
$$

This is rewritten in matrix form as

$$
\{\varepsilon^e\} = [B^e]\{d^e\}, \tag{3.29}
$$

where $[B^e]$ is a 3×6-element matrix in the right-hand side of (3.23) and $\{d^e\}$ represents the displacement vector, a 6×1 column matrix having six degrees of freedom for $e^{th}$ element, i.e.,

$$
[B^e] = \frac{1}{2s_e} \begin{bmatrix} (y_j - y_k) & 0 & (y_k - y_j) & 0 & (y_i - y_j) & 0 \\ 0 & (x_k - x_j) & 0 & (x_i - x_k) & 0 & (x_j - x_i) \\ (x_k - x_j) & (y_j - y_k) & (x_i - x_k) & (y_k - y_i) & (x_j - x_i) & (y_i - y_j) \end{bmatrix}, \tag{3.30}
$$

and

$$
\{d^e\} = \begin{bmatrix} u_i \\ v_i \\ u_j \\ v_j \\ u_k \\ v_k \end{bmatrix}. \tag{3.31}
$$

The strain energy in the eth element is then expressed as

$$
U^e = \frac{1}{2} \iint \{\sigma^e\}^T \left[ \{\varepsilon^e\} - \{\varepsilon_0^e\} \right] dx\, dy. \tag{3.32}
$$

From (3.15), $\{\sigma^e\}^T$ of (3.26) can be expressed as

$$
\{\sigma^e\}^T = \left[ \{\varepsilon^e\}^T - \{\varepsilon_0^e\}^T \right] [D^e]^T = \left[ \{d^e\}^T [B^e]^T - \{\varepsilon_0^e\}^T \right] [D^e]^T \tag{3.33}
$$

Here, $\left[ D^e \right] \equiv \left[ D^e \right]^T$ and the element matrix $\left[ D^e \right]$ may be different in each element, since the Young's modulus and the Poisson's ratio are different in different materials (the core and substrate regions). Also, note that if $[A] = [B][C]$, then $[A]^T = [C]^T [B]^T$. Now, using (3.27), (3.26) can be expressed as

$$U^e = \frac{1}{2} \iint\limits_e \left( \begin{array}{c} \{d^e\}^T \left[ B^e \right]^T \left[ D^e \right]^T \left[ B^e \right] \{d^e\} \quad - \\ 2\{d^e\}^T \left[ B^e \right]^T \left[ D^e \right]^T \{\varepsilon_0^e\} \quad + \quad \{\varepsilon_0^e\}^T \left[ D^e \right]^T \{\varepsilon_0^e\} \end{array} \right) dx\, dy$$

$$= \frac{s_e}{2} \left( \{d^e\}^T \left[ B^e \right]^T \left[ D^e \right]^T \left[ B^e \right] \{d^e\} - 2\{d^e\}^T \left[ B^e \right]^T \left[ D^e \right]^T \{\varepsilon_0^e\} + \{\varepsilon_0^e\}^T \left[ D^e \right]^T \{\varepsilon_0^e\} \right) \quad (3.34)$$

For the last term of the above equation, we can find that

$$\{\varepsilon_0^e\}^T \left[ D^e \right]^T \{\varepsilon_0^e\} = \frac{2(1+\mu_e)E_e}{(1-2\mu_e)} \; (\alpha_e \Delta T)^2 . \tag{3.35}$$

Here $E_e$, $\mu_e$, and $\alpha_e$ are the Young's modulus, the Poisson's ratio, and the thermal expansion coefficient of the element. Since (3.28) is always positive, it can be neglected in the minimization process of potential energy. Then the strain energy $U^e$ in the eth element is expressed as

$$U^e = \frac{1}{2} \{d^e\}^T \left[ A^e \right] \{d^e\} - \{d^e\}^T \{h^e\} . \tag{3.36}$$

Here $[A^e]$ is a 6×6-element stiffness matrix and $\{h^e\}$ is a 6×1 thermal stress vector, which are given by

$$\left[ A^e \right] = s_e \left[ B^e \right]^T \left[ D^e \right]^T \left[ B^e \right], \tag{3.37}$$

and

$$\{h^e\} = s_e \left[ B^e \right]^T \left[ D^e \right]^T \{\varepsilon_0^e\} . \tag{3.38}$$

The total strain energy is then obtained by summing the element strain energy:

$$U = \sum_{e=1}^{N} U^e = \frac{1}{2} \{d\}^T [A]\{d\} - \{d\}^T \{H\}, \tag{3.39}$$

Where $\{d\}$, $[A]$, and $\{H\}$ are the 2n×1 global strain vector, the 2n×2n global stiffness matrix, and the 2n×1 global thermal stress vector, respectively.

An external force applied to the body is approximated by the force concentrated at the node on the surface of the body. Then the vector of the external force is expressed by

30

$$\left\{ f_L{}' \right\} = \begin{bmatrix} f_1 \\ g_1 \\ f_2 \\ g_2 \\ \vdots \\ f_n \\ g_n \end{bmatrix}, \qquad (3.40)$$

where n is the number of nodes on the surface of the body, $f_i$ and $g_i$ denote the x- and y-axis components of the external force applied to nodal point i. When a displacement ($u_i$, $v_i$) is generated by the external force ($f_i$, $g_i$), the work done by the force is ($u_i f_i + v_i g_i$). The total work done by the external force is then given by

$$V' = \{d'\}^T \left\{ f_L{}' \right\} \qquad (3.41)$$

Here $\{d'\}$ is the displacement vector comprised of $u_i$'s and $v_i$'s of n nodes on the surface under stress. However, in order to add up the energy of the external force to the total potential energy, we have to find the work done from all the nodal contributions such that

$$V = \{d\}^T \{f_L\} \qquad (3.42)$$

where, in finding V, the force on nodes other than the nodes on surface must be zero, so that V=V'. Therefore, $\{f_L\}$ is the global load vector acting on each nodal point.

Now, the total potential energy is given by

$$\Pi = U - V = \frac{1}{2}\{d\}^T [A]\{d\} - \{d\}^T \big[ \{H\} + \{f_L\} \big]. \qquad (3.43)$$

For the thermal stress analysis of birefringent fibers and waveguides without external force, we simply make $\{f_L\} = \{0\}$.

Potential energy should be a minimum by the energy principle. Therefore, the partial derivative of $\Pi$ with respect to the displacement of each nodal point should be zero: i.e.,

$$\frac{\partial \Pi}{\partial \{d\}} = [A]\{d\} - \{H\} - \{f_L\} = 0. \qquad (3.44)$$

We then have the 2nd-order linear simultaneous equations:

$$[A]\{d\} = \{H\} + \{f_L\}.$$ (3.45)

For the global system, now it can be written that

$$[A] = \sum_{e=1}^{N} \iint_e [B^e]^T [D^e][B^e] \, dx \, dy,$$ (3.46)

$$\{H\} = \sum_{e=1}^{N} \iint_e [B^e]^T [D^e]\{\varepsilon_0^e\} \, dx \, dy.$$ (3.47)

The solution of (3.36) gives the displacements at all nodal points of the fiber or waveguide under thermal stress and/or external forces. The solution of the displacement vector can be easily obtained as:

$$\{d\} = [A]^{-1} \left[ \{H\} + \{f_L\} \right].$$ (3.48)

General sparse matrix solver may be employed to solve the system of linear simultaneous equations in order to find the displacement vector. Once the displacement of each node is known, the stress in each element is calculated by

$$\{\sigma^e\} = [D^e] \left( [B^e]\{d^e\} - \{\varepsilon_0^e\} \right). \quad (e = 1\text{---}N).$$ (3.49)

However, in solving the linear simultaneous equations, the boundary conditions should be taken into account very carefully. Also, symmetry conditions can be used to reduce memory and time of computation in the case of finite element analysis.

In optical fibers or waveguides under stress or strain, the original refractive index of the material changes due to the photoelastic effect. The new refractive index for x- and y-polarized light can be calculated from the equation as:.

$$\begin{bmatrix} n_x(x,y) \\ n_y(x,y) \\ n_z(x,y) \end{bmatrix} = \begin{bmatrix} n_{x0}(x,y) \\ n_{y0}(x,y) \\ n_{z0}(x,y) \end{bmatrix} - \begin{bmatrix} C_1 & C_2 & C_2 \\ C_2 & C_1 & C_2 \\ C_2 & C_2 & C_1 \end{bmatrix} \begin{bmatrix} \sigma_x(x,y) \\ \sigma_y(x,y) \\ \sigma_z(x,y) \end{bmatrix}.$$ (3.50)

Here, $C_1$, $C_2$ are the elasto-optic (photo elastic) coefficients of the fiber or waveguide material, $n_{x0}$, $n_{y0}$, and $n_{z0}$ are the unstressed refractive indices of the material and $n_x$, $n_y$, and $n_z$ are the main diagonal

elements of the anisotropic refractive index tensor. Since the material considered here is silica, an isotropic material for the fiber, having a refractive index, n, we have in this case

$$n_{x0}(x, y) = n_{y0}(x, y) = n_{z0}(x, y) = n \qquad (3.51)$$

Once the stress analysis is performed, the anisotropic refractive index components can be calculated. Thus, the refractive index distribution over the cross-section of the fiber under stress is known. Therefore, the vector finite element method can then be employed to find the modal solutions of quasi-TE ($H_{11}^y$) and quasi-TM ($H_{11}^x$) modes. The details of the vector FEM can be found in the literature.

## 3.4 Analysis of PCF using COMSOL Multiphysics

Numerical software is playing an important role in the design of single mode waveguides and fibers. To summarize in general terms how the multiphysics works we list main steps of the procedure below.

### 3.4.1 Modeling of PCF without Stress using COMSOL Multiphysics

COMSOL Multiphysics has been used here for modeling of PCF made of silica with a refractive index $n_{co}$ = 1.4440 and the cladding is an array of periodically arranged air holes lattice that makes an effective refractive index, $n_{eff}$. These values are valid for free space wavelengths of 1.55 μm. In holey fiber (HF), the core index is greater than the average index of the cladding because of the presence of the air holes, and the fiber can guide light (mode) by total internal reflection as conventional step-index fiber does. That is, guided light has an effective index, $n_{eff}$, which satisfies the condition :

$$n_{co} \rangle n_{eff} = \frac{\beta}{k_0} \rangle n_{FSM} \qquad (3.52)$$

where, $\beta$ is the propagation constant along the fiber axis, $k_0$ is the free-space wave number, $n_{co}$ is the core index, and $n_{FSM}$ is the cladding effective index of the fundamental space-filling mode (FSM) of the infinite photonic crystal cladding if the core is absent. In the case of HF made from pure silica, the $n_{co}$ is reduced to the index of silica.

The waves are mode confined when $n_{eff}$ is close to the upper limit in this interval. The mode analysis is made on a cross-section in the x-y plane of the fiber. The wave propagates in the z direction and has the form

$$\mathbf{H}(x,y,z,t) = \mathbf{H}(x,y)e^{j(\omega t - \beta z)} \tag{3.53}$$

where, $\omega$ is the angular frequency and $\beta$ the z component of propagation constant. An eigenvalue equation for the magnetic field H is derived from Helmholtz equation

$$\nabla \times (n^{-2} \nabla \times \mathbf{H}) - k_0^2 \, \mathbf{H} = 0 \tag{3.54}$$

which is solved for the eigenvalue $\lambda = -\beta^2$.

As the boundary condition along the outside of the cladding the magnetic field is set to zero. Because the amplitude of the field decays rapidly as a function of the radius of the cladding this is a valid boundary condition.

When studying the characteristics of optical fibers, effective mode index of a confined mode,

$$n_{eff} = \frac{\beta}{k_0} \tag{3.55}$$

as a function of the frequency is an important characteristic.

## Modeling using the Graphical User Interface

**Model Navigator**

In the Model Navigator, select 2D in Space dimension list.

1. Select the Electromagnetic Module>Perpendicular Waves>Hybrid-Mode Waves>Mode Analysis Application Mode.

2. Write hx hy hz and emwv (perpendicular hybrid mode wave) in Dependent variables and Application mode name dialog box.

3. Select Vector,Lagrange- Quadratic in Element list.

4. Click OK.

**Application Mode Properties**

1. Select Physics > Properties.

2. In the Application Mode Properties dialog box, set the Default Element Type to Lagrange-Quadratic.

3. Set the Analysis Type to Mode Analysis.

4. Set the Field Type to Hybrid-Mode Waves.

5. For convenience, set the property Specify Wave Using to Free Space Wavelength. This makes the wavelength available in the Application Scalar Variables dialog box instead of the frequency.

6. Set Field Components to In-plane Components. This selects the two components equation formulation for hybrid-mode waves.

7. Set the Specify Eigenvalue Using to Effective Mode Index.

## <u>Options and Settings</u>

In the Constant dialog box, enter the following names and expressions for the refractive indices.

**Table 3.1 : Constants (refractive index)**

| Name | Expression |
|------|------------|
| $n_{Hole}$ | 1.0 |
| $n_{Clad}$ | 1.4440 |

**Geometry Modeling**

1. A PCF with 4 (four) layers of air hole rings periodically arranged in a symmetric lattice of air holes concentric with another bigger circle centered at (0,0) is drawn.

2. Click the Zoom Extents button for a full visualization.

## Physics Settings (scalar variables)

In the Application Scalar Variables dialog box, the free space wavelength lambda0_emwv to 1.55 μm is set.

## Boundary Settings

**Equation:**  $\mathbf{n} \times (\mathbf{H}_1 - \mathbf{H}_2) = 0, \mathbf{n} \times (\mathbf{E}_1 - \mathbf{E}_2) = 0$ (3.56)

Set the exterior boundary condition to perfect magnetic conductor and Interior boundary condition to continuity.

## Subdomain Settings

### Equation

$$\nabla \times (n^{-2} \nabla \times \mathbf{H}) - k_0 \mathbf{H} = 0, \mathbf{H} = \mathbf{H}(x,y)\exp(-j\beta z), \varepsilon_r = n^2, \mu_r = 1, \sigma = 0, \lambda = -\beta^2 \qquad (3.57)$$

In the Subdomain Settings dialog box select the Physics tab. Select 'Specify Material Properties' in Terms of Refractive Index and write the refractive index in 'n(isotropic)' dialog box for the subdomain 1 (hole) and 2 (clad).

### Mesh Generation

1. Initialize the mesh.
2. Refine the mesh.

### Computing the Solution

The modes of interest have an effective mode index somewhere between the refractive indices of the solid core and the microstructured cladding, that is,

$$1.4440 < n_{\text{eff}} < 1.523$$

1. In the Solver parameter dialog box set the parameter Search for effective mode indices around to 1.46. This guarantees that the solver will find the fundamental mode, which has the largest effective mode index. If we set $n_{\text{eff}} < 1.46$ then Unguided or Radiation mode and Leaky mode are found.
2. Solve the problem.

## <u>Post Processing and Visualization</u>

The default plot shows the power flow in the z direction for the fundamental mode. This is $HE_{11}$ mode which is verified by visualizing the transversal components of both the magnetic and the electric field. To visualize the other mode select the General tab of Postprocessing in the Plot Parameter dialog box. Select effective mode index from the list. Various plots (e.g. surface plot, contour plot, displacement) can be shown by selecting Predefined Quantities (e.g. electric field, magnetic field, power flow).

To view the electric field, x component or y component or power flow along a horizontal line through the entire structure, use a cross-section plot. In the Cross-Section Plot Parameters dialog box, select the desired quantities as y-axis data on the Line/Extrusion tab. As Cross-section line data set x0 to -50e-6, y0 to 0, x1 to 50e-6, y1 to 0. Use x as x-axis data.

## 3.4.2 Modeling of PCF with Thermal Stress

Anisotropic refractive indices result in fundamental mode splitting and pulse broadening. Anisotropic refractive indices can be achieved by applying thermal stress which causes birefringence. The source of birefringence is the use of two types of material (air and silica) having different thermal expansivity as core and clad. After annealing at high temperature (approximately 1000°C), mismatch in thermal expansivity between the core and clad results in thermal induced stresses in the structure at the operating temperature (typically room temperature, 20°C).

## 3.4.3  The Stress-Optical Effect and Plane Strain

The general linear stress-optical relation can be written, using tensor notation, as

$$\Delta n_{ij} = - B_{ijkl} \sigma_{kl} \tag{3.58}$$

where, $\Delta n_{ij} = n_{ij} - n_o I_{jk}$, $n_{ij}$ is the refractive index tensor, $n_o$ is the refractive index for a stress free material, $I_{jk}$ is the identity tensor, $B_{ijkl}$ is the stress-optical tensor, and $\sigma_{kl}$ is the stress tensor. Due to symmetry the number of independent parameters in the stress optical tensor that characterizes this constitutive relation can be reduced. Since $n_{ij}$ and $\sigma_{kl}$ are both symmetric, $B_{ijkl} = B_{jikl}$ and $B_{ijkl} = B_{ijlk}$. In many cases the number of independent parameters can be further reduced and in this model only two independent parameters can be further reduced and in this model only two independent parameters, $B_1$ and $B_2$, will be used. The stress-optical relation simplifies to

$$\begin{bmatrix} \Delta n_x \\ \Delta n_y \\ \Delta n_z \end{bmatrix} = \begin{bmatrix} B_2 & B_1 & B_1 \\ B_1 & B_2 & B_1 \\ B_1 & B_1 & B_2 \end{bmatrix} \begin{bmatrix} \sigma_x \\ \sigma_y \\ \sigma_z \end{bmatrix} \tag{3.59}$$

where, $n_x = n_{11}$, $n_y = n_{22}$, $n_z = n_{33}$, $\sigma_x = \sigma_{11}$, $\sigma_y = \sigma_{22}$, $\sigma_z = \sigma_{33}$. This translates to

$$n_x = n_0 - B_2 \, \sigma_x - B_1 \, (\sigma_y + \sigma_z)$$

$$n_y = n_0 - B_2 \, \sigma_y - B_1 \, (\sigma_x + \sigma_z)$$

$$n_z = n_0 - B_2 \, \sigma_z - B_1 \, (\sigma_y + \sigma_x) \qquad (3.60)$$

Using the two parameters $B_1$ and $B_2$, it is assumed that the non-diagonal parts of $n_{ij}$ and $\sigma_{kl}$ are negligible. This means that the shear stress corresponding to $\sigma_{12} = \tau_{xy}$ is neglected. In addition, the shear stress corresponding to $\sigma_{13} = \tau_{xz}$ and $\sigma_{23} = \tau_{yz}$ are neglected by using the plain strain approximation. The plain strain approximation holds in a situation where the structure is free in the x and y direction but where the z strain is assumed to be zero. Note that this deformation state is not correct if the structure is also free in z direction. In such a case a modified deformation state equation is needed where the x and z directions are equivalently handled. The first part of this model utilizes the plain strain application mode of the Structural Mechanics Module. The resulting birefringent index is computed using expression variables and can be considered a post processing step of the plain strain model. The refractive index tensor is used as material data for the second part of the model, the mode analysis.

## Perpendicular Hybrid Mode Waves

For a given frequency ν, or equivalently, free space wavelength $\lambda_0 = c_0/\nu$, the perpendicular hybrid mode waves application mode of the Electromagnetic Module can be used for the mode analysis. In this model the free-space wavelength is chosen 1.55 μm. The simulation is set up with the normalized magnetic field components $\mathbf{H} = (\mathbf{H}_x, \mathbf{H}_y, \mathbf{H}_z)$ as dependent variables and the effective mode index $n_{eff} = \beta/k_0$ is obtained from the eigenvalues.

Using the application mode, the wave is assumed to have the form

$$\mathbf{H} = \mathbf{H}(x, y)e^{j(\varpi t - \beta z)} = (\mathbf{H}_x(x, y), \mathbf{H}_y(x, y), \mathbf{H}_z(x, y)e^{j(\varpi t - \beta z)}) \qquad (3.61)$$

The computation will show a shift in effective mode index due to the stress induced change in refractive index. The birefringence will cause the otherwise two-fold degenerate fundamental mode to split.

## Plane Strain Analysis

1. Select the Structural Mechanics Module>Plain Strain>Static Analysis application mode.

2. Write u v p in Dependent variables dialog box and smpn in Application mode name dialog box. Select Lagrange-Quadratic in Element list.

3. Click Multiphysics then Add to add this application mode to the model.

4. Next select the Electromagnetic Module>Perpendicular Waves>Hybrid-Mode Waves>Mode Analysis application mode. Add this mode to the model.

5. Write hx2 hy2 hz2 in Dependent Variables dialog box and emwv2 in Application Mode Name dialog box. Select Vector, Lagrange-Quadratic in Element list.

6. Open the Application Mode Properties dialog box and set Default Element Type to Vector, Lagrange-Quadratic.

7. Set Analysis Type to Mode Analysis.

8. Set Field Type Hybrid-mode Waves.

9. For convenience set the property Specify Wave Using to Free Space Wavelength. This makes the wavelength available in the Application Scalar Variables dialog box instead of the frequency.

10. Set Solve For to Magnetic Field.

11. Set Field Components to In-plane Components. This selects the two-component equation formulation for hybrid-mode waves.

12. Set the Specify Eigenvalues Using to Effective Mode Index.

13. Set the Ruling Application Mode to the Perpendicular Hybrid-Mode Waves (emwv) application mode. This makes this mode specify the interpretation of the parameters to the eigenvalue solver given in the Solver Parameters dialog box.

## Options and Settings

In the Constant Dialog Box, enter the following names and expressions.

### Table 3.2 Constant dialog box

| Name | Expression | Description |
| --- | --- | --- |
| $n_{Hole}$ | 1.0 | Refractive index, air hole |
| $n_{Clad}$ | 1.4440 | Refractive index, silica ($SiO_2$) |
| deltan | $\Delta = \dfrac{(n_{core}^2 - n_{clad}^2)}{2n_{core}^2}$ | Relative index difference |
| alphaSiO2, $\alpha_1$ | 1e-6 | Thermal expansion coefficient, silica ($K^{-1}$) |
| alphaair, $\alpha_2$ | 1.49e-3 | Thermal expansion coefficient, air ($K^{-1}$) |
| Eair | 1.43e5 | Young's Modulus, air ($N/m^2$) |
| ESiO2 | 78e9 | Young's mod, silica |
| nuSiO2 | 0.42 | Poisson's ratio, silica |
| nuair | 0.33 | Poisson's ratio, air |
| $B_1$ | $4.18 \times 10^{-12}$ | First Stress optical coefficient ($m^2/N$) |
| $B_2$ | $7.5714 \times 10^{-13}$ | Second Stress optical Coefficient ($m^2/N$) |
| $T_1$ | 20 | Operating temperature (°C) |
| $T_2$ | 1000 | Reference temperature (°C) |

Notice that the temperatures are given in degrees celcius (°c). This works well since this is a linear model. (Nonlinear model needs to have temperatures in Kelvin to get the correct thermodynamics).

## Geometry Modeling

The PCF as described in 3.4.1 is drawn.

## Physics Settings

## Point Settings and Boundary Conditions

All regions have free boundaries, which also is the default boundary condition. However, these conditions will not suffice in creating a unique solution since the computational domain is allowed to move and rotate freely; the problem is ill-posed. The problem becomes well-posed by adding constraints at points to keep the domain fixed according to the following steps:

1. From the Multiphysics menu the Plain Strain application mode is selected.

2. From the Point Settings dialog box in Physics menu, and checking the constraints $R_x$ at points 3, 4, 5 and 6 along the y axis, keeping the domain from rotating but allowing it to slide in the y direction.

3. Checking the constraints $R_y$ at points 1, 2, 7 and 8 along x axis, keeping the domain from rotating but allowing it to slide in the x direction.

**Sub domain Settings**

The Subdomain Settings in Physics menu for the Plain Strain application mode is specified according to the following table:

**Table 3.3 Sub domain settings**

| Sub domain | 1 | Parameter | 1 | | 2 to all air holes (61) | Parameter | 2 to all air holes (61) | |
|---|---|---|---|---|---|---|---|---|
| Tab | Material | | Loads | | Material | | Loads | |
| | E | ESiO2 | | | E | Eair | | |
| | v | nuSiO2 | Temp | $T_1$ | v | nuair | Temp | $T_1$ |
| | α | alphaSiO2 | Tempref | $T_o$ | α | alphaair | Tempref | $T_o$ |

The other material parameters density ρ, thickness m, mass damping parameter $\alpha_{dM}$ and stiffness damping parameter $\beta_{dK}$, need not be specified because they do not enter the equation for static problem.

**Expression Variables**

In the Subdomain Expression dialog box in the Option menu, define the following variables:

**Table 3.4 Expression variables**

| Variable Name | Subdomain | Expression |
|---|---|---|
| N | 1 | $n_{Clad}$ |
| | 2, 3, ---- | $n_{Hole}$ |
| Nx | 1,2,3,--- | $N-B_1*sx\_smpn-B_2*(sy\_smpn+sz\_smpn)$ |
| Ny | 1,2,3,--- | $N-B_1*sy\_smpn-B_2*(sx\_smpn+sz\_smpn)$ |
| Nz | 1,2,3,--- | $N-B_1*sz\_smpn-B_2*(sx\_smpn+sy\_smpn)$ |

## 3.4.4 Modeling of PCF with Thermal & External Stress

To apply the external stress, follow the steps below

1. From Multiphysics menu the Plain Strain application mode is to be selected.
2. In the Physics menu, the Load tab is to be selected from the Boundary Settings dialog box.
3. In the Boundary Selection box, the exterior boundary (boundary 1, 2, 5 & 8) is selected
4. "Edge load is defined as force/length " is to be selected.
5. The values of edge load along x direction and y direction are to be inserted in the $F_x$ and $F_y$ dialog box respectively.

### Mesh Generation

The fiber cross section is divided into small elements by initializing a mesh and refining it.

### Computing the Solution

1. In the Solver Parameter dialog box Stationary Linear for Solver to be selected.
2. Direct (UMFPACK) in the Linear System Solver dialog box and Nonsymmetric in Matrix Symmetry dialog box to be selected.
3. On the Solve For tab in the Solver Manager dialog box, only the Plane Strain application mode to be selected. This will make sure that only the Plane Strain application mode equations are solved in the first run.
4. "Initial value expression evaluated using current solution" is to be selected in the Initial Value tab.
5. Then the Solve button clicked.

### Postprocessing and Visualization

The default plot shows the Von Mices effective stress as a colored surface plot.

1. To view the stress induced birefringence, type Nx-Ny as Surface data in the Plot Parameter dialog box.
2. Now create a cross-section plot of the birefringence Nx-Ny on the horizontal line from (-10 μm, 0) to (10 μm, 0). It is to be done by entering Nx-Ny as y axis data, and setting $x_o$ to -10 μm, $y_o$ to 0, $x_1$ to 10 μm in cross-section plot parameters dialog box. The x axis data is to be set as x in place of arc length.

# Optical Mode Analysis

From the Multiphysics menu the Perpendicular Hybrid-Mode Waves (emwv) application mode is to be selected.

## Physics Setting : Scalar Variables

In the Application Scalar Variables dialog box, the free space wavelength is to be selected to 1.55 μm. Wavelength can be changed by putting another values. In that case corresponding refractive indices must be written in the constant dialog box which can be calculated using Sellmeier equation.

## Subdomain Settings

For all domains, select n (anisotropic) and set Nx, Ny, and Nz, respectively, as anisotropic refractive indices by changing the entries on the diagonal in the refractive index matrix.

## Boundary Conditions

Same as 3.4.2.

## Mesh Generator

Mesh density can be changed by changing the values of Maximum Element Size on the Subdomain tab in the Mesh Parameters dialog box.

## Computing the Solution

1. In the Solver Parameters dialog box, the Eigenvalue solver is to be selected.

2. In the "Search for effective indices around" box the value is to be written greater or equal to $n_1$. The default "Desired Number of Effective Indices" is set to 6, which is changed up to 14 in this work. These settings will make the eigenvalue solver search for the 14 eigenmodes with effective mode indices closest to the value $n_1$. This value is an estimate of the effective mode index for the fundamental mode. For propagating modes it must hold that $n_{eff} < n_1$.

3. In the Solver Manager dialog box, only the Perpendicular Hybrid-Mode Waves application mode is to be selected on the Solve For tab. This will ensure that the Plane Strain application mode will not be part of the eigenmode computation.

4. On the Initial Value tab, the initial value to Current Solution is to be selected. This will take the Plane Strain solution and use it to evaluate the refractive indices for the mode analysis.

5. Now, the Solve button is to be clicked.

Although the fundamental mode have converged to 5 decimal places the known modeling errors makes the exactness of the numbers uncertain. One major modeling error is due to the fact that we used plain strain in a case where the real world model does not necessarily conform to this deformation state. Moreover, the material properties are only known to a few decimal places and the computed magnitudes of the effective mode indices will correspondingly be uncertain. A standard way of examining the effects of uncertainty in material parameters is to perform a sensitivity analysis. That is, one of the material parameters is slightly perturbed and the resulting perturbation in the computed parameter is examined. Another source of uncertainty is whether the thermal expansion is large with respect to the other sources of stress in the material originating from the manufacturing process.

# CHAPTER 4

# Results and Discussion

The aim of this chapter is to show numerical results obtained in this work by using the finite element method. To carry out the optical analysis for determining the modal characteristics, the COMSOL Metaphysics [31] as discussed in the previous chapter is employed. Structural mechanics module is used to carry out the stress analysis of PCF. As the refraction index of the fiber material changes due to stress-optic effect, the new refraction index is calculated after the stress analysis is finished. Then modal analysis of the fiber with the new refractive index is carried out using the electromagnetic module. In the process, at the very outset, the model has been verified for its applicability and correctness by investigating a few parameters of an unstressed PCF and comparing the results with the same exhibited in [10]. Thereafter, modal analysis has been carried out to analyze the effect of stress on various optical properties, e.g. birefringence, modal confinement, dispersion, polarization mode dispersion, effective mode area etc. of a PCF. The influence of core shape and size and the number of the layers of air hole rings have also been addressed in this work. Also, the wavelength dependence of all these properties of PCF under external stress will be investigated.

## 4.1 Modal Solution of Solid Core PCF

Fig. 4.1 shows the schematic diagram of the full cross section of a PCF, consisting of two rings of arrays of air holes (total 18 air-holes) arranged in a silica background whose refractive index has been taken as 1.45 at a wave length of 1550 nm. In the geometry shown, d is the hole diameter and $\Lambda$ is the hole pitch of the PCF. It is assumed that the PCF is uniform in the longitudinal direction.

Fig. 4.2 shows the 3D as well as plot of time average power flow in an unstressed (P=0) PCF with two rings of air holes. The figure here shows the fundamental mode, $HE_{11}$ mode, supported by the fiber. As expected the modal spot is confined in the central core region. The maximum power flow, as observed from the plot information is 4399.714 W/m$^2$ at wavelength 1550 nm

while the minimum power flow is -6.047 W/m². The corresponding electric field and magnetic field distributions are shown in Fig. 4.3 both in vector and contour form.
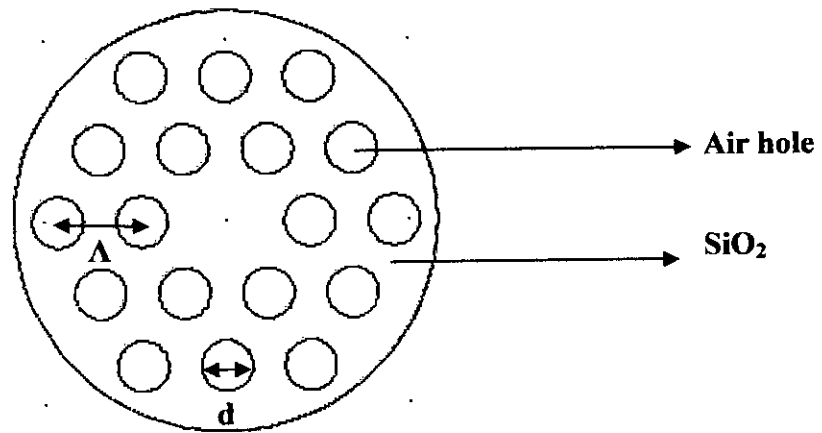


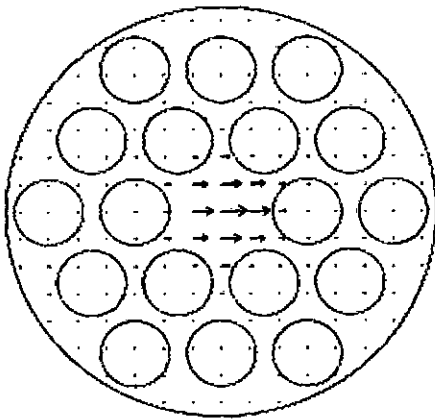Fig. 4.1 : Schematic diagram of the cross section of a Two Ring PCF



(a) 3D plot

(b) Surface plot
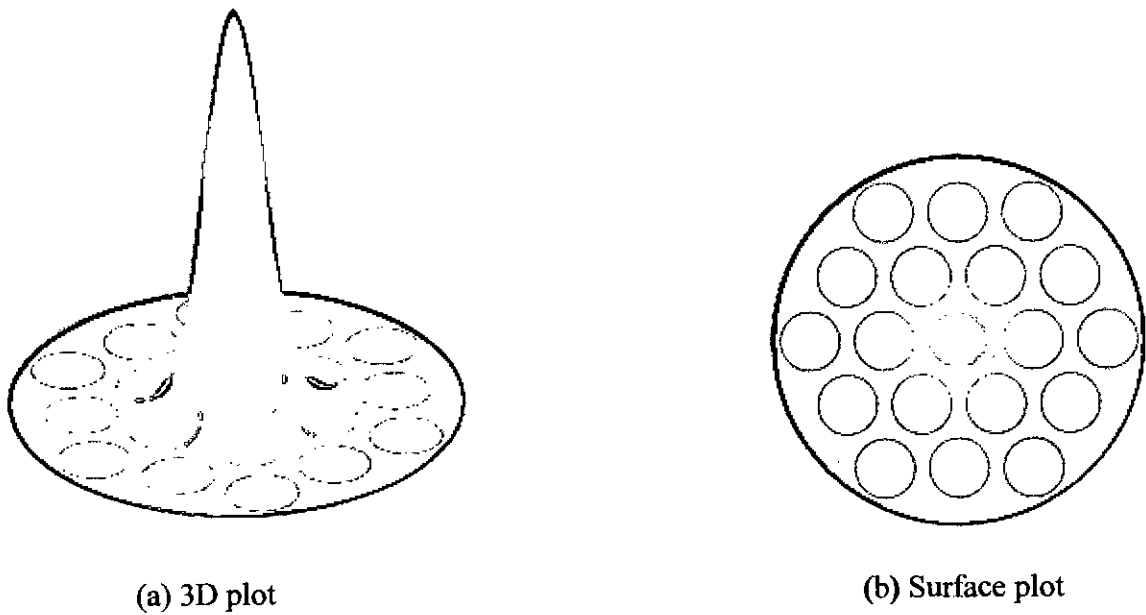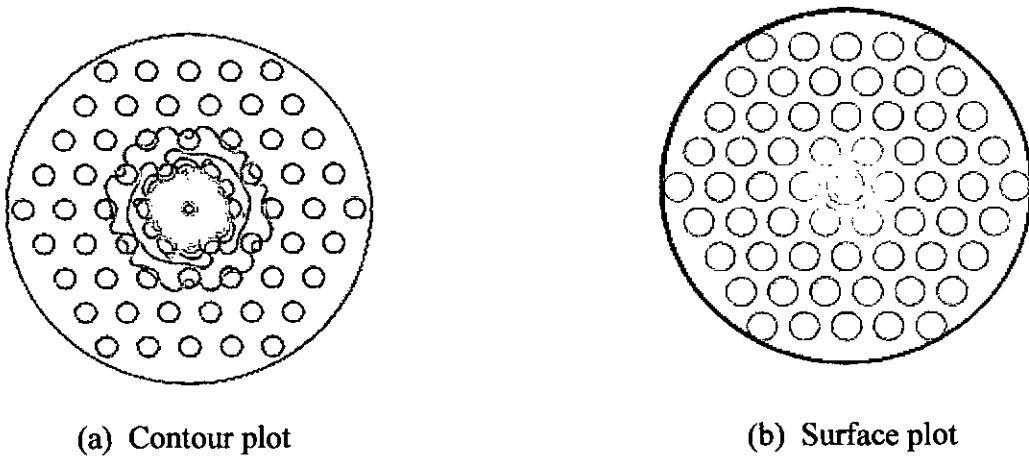
Fig. 4.2 : Power flow (time average, z component) in a two ring PCF with d=0.6 μm, Λ=1.2 μm
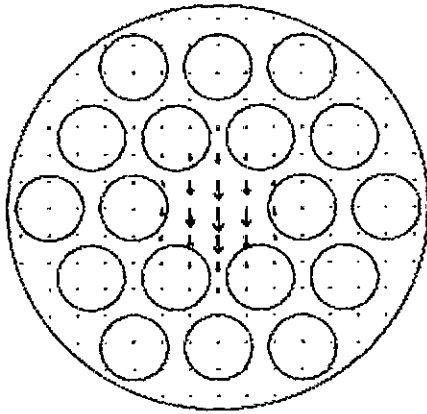
(a) dominant electric field (vector plot)
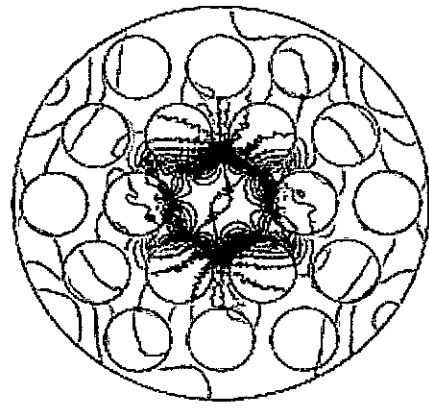


(b) dominant electric field (contour plot)



(a) dominant magnetic field (vector plot)
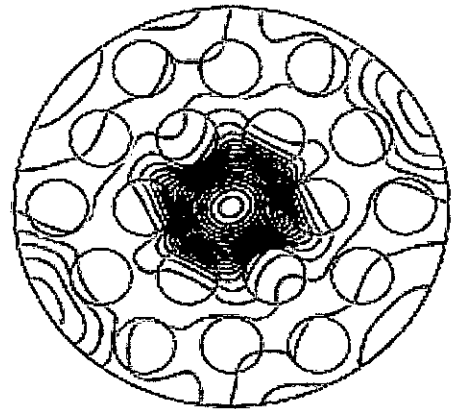


(b) dominant magnetic field (contour plot)

Fig. 4.3 : Field distribution of the fundamental $x$-polarized mode in a two ring PCF with d=0.6 μm and $\Lambda$=1.2 μm

For two rings of 18 air holes, Fig. 4.4 shows the variation of the effective index with the pitch $\Lambda$, where the ratio d/$\Lambda$ is taken as a parameter. Here the solid line, dashed line, dashed-dotted line, and the dotted line show the results for d/$\Lambda$ = 0.6, 0.7, 0.8 and 0.9, respectively. The dark circles show the results of Obayya et. al. [10]. It can be seen that our results agree well with those of Obayya et. al. for a two ring PCF. As may be observed from Fig. 4.4, the effective index of the fundamental mode increases monotonically with the increase of the hole pitch, $\Lambda$ or the decrease in the ratio d/$\Lambda$.
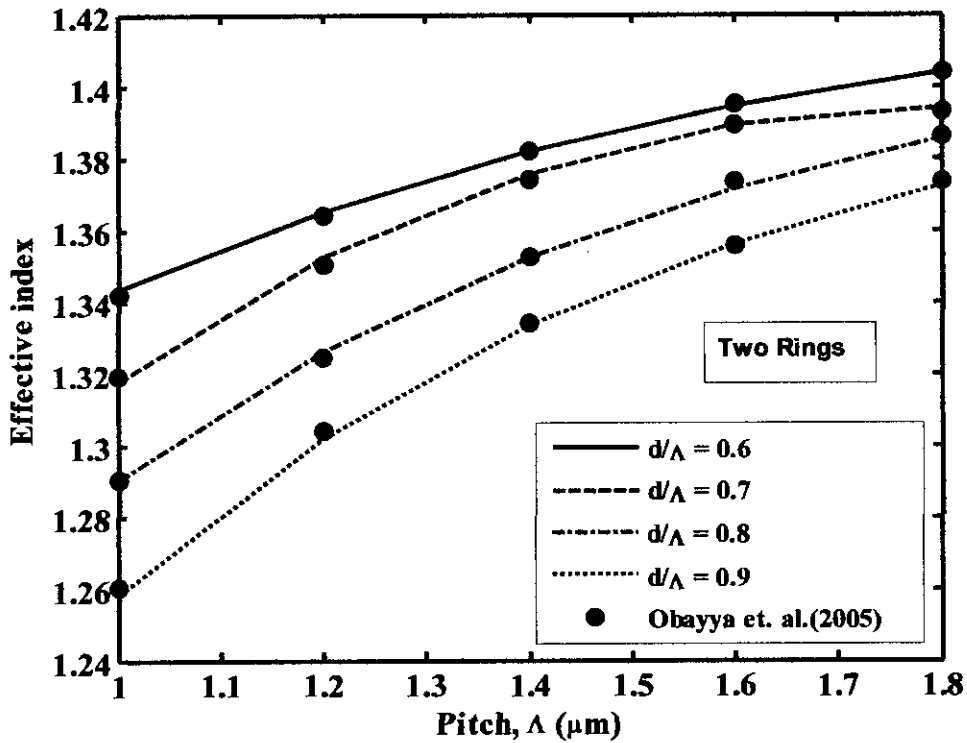
Fig. 4.4 : Variation of the effective index of a two-ring PCF taking d/Λ as parameter.

Fig. 4.5 shows the plot of power flow (time average, z component), in an unstressed (P=0) PCF with four rings of air holes. The figure here shows the fundamental mode, $HE_{11}$ mode, supported by the fiber. As expected the modal spot is confined in the central core region. The maximum power flow, as observed from the plot information is 9667.001 $W/m^2$ at wavelength 1550 nm while the minimum power flow is -0.0101 $W/m^2$. The corresponding electric field and magnetic field distributions are shown in Fig. 4.6 both in vector and contour form.



| (a) Contour plot | (b) Surface plot |

Fig. 4.5 : Plot of power flow (time average, z component) in a four-ring PCF when Λ=1.0 µm and d/Λ =0 .5
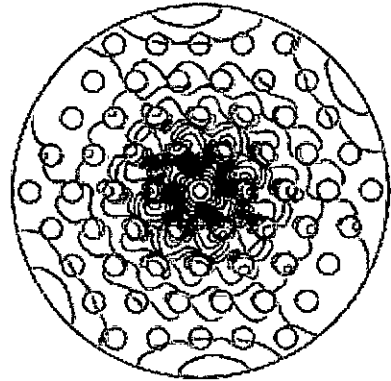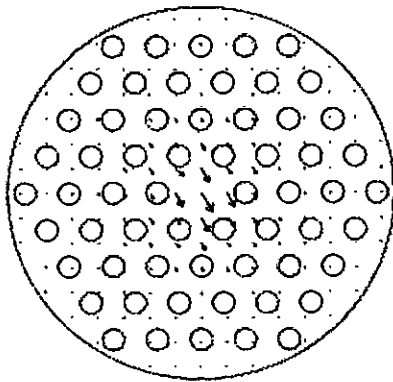
(a) vector plot of electric field distribution   (b) Contour plot of electric field distribution
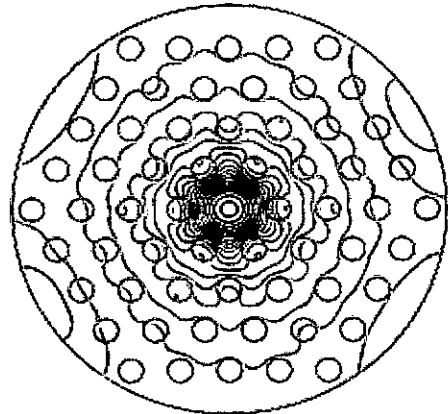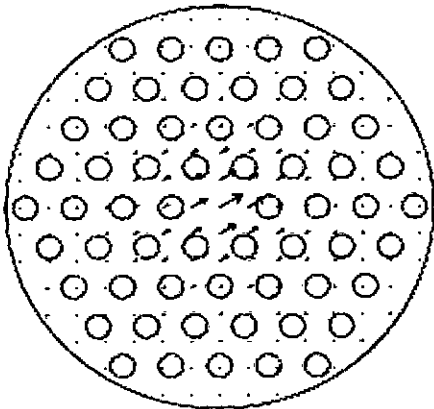
(a) vector plot of magnetic field distribution      (b) Contour plot of magnetic field distribution

Fig. 4.6 : Distribution of dominant electric and magnetic fields in a four-ring PCF with $\Lambda$=1.0 μm and d/$\Lambda$ =0 .5:
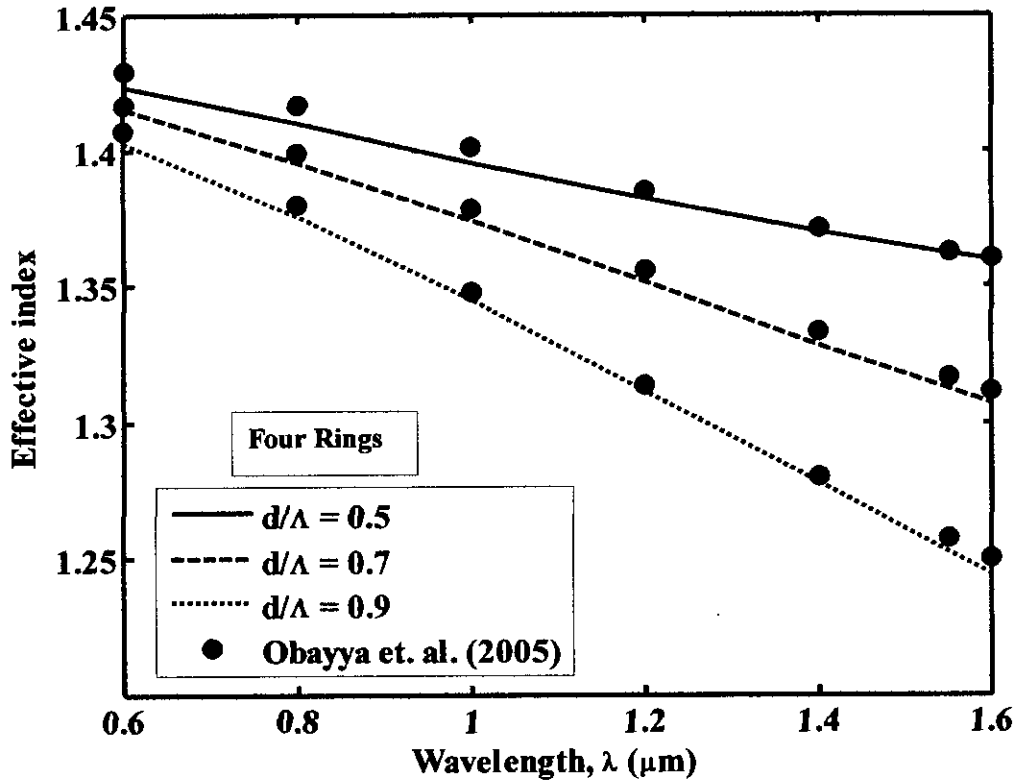
Fig. 4.7 : Variation of the effective index of a four-ring PCF with hole pitch, $\Lambda$=1.0 μm with wavelength, $\lambda$ as parameter

Again, the Fig. 4.7 shows the effective index, $n_{eff}$ versus wavelength, $\lambda$ for different values of d/$\Lambda$ for a specific geometrical structure of PCF (4 rings of air holes with $\Lambda$ = 1.0 μm). It may be noted from the figure that the effective index steadily decreases as the wave length is increased. Therefore, it is evident from the figure that at shorter wavelengths the mode tends to be more confined, while at longer wavelengths the mode becomes less confined to the core region. Here also the calculated results are compared with the same of [10]. Here the solid line, dashed line, and the dotted line show the results for d/$\Lambda$ = 0.5, 0.7, 0.9 respectively. The dark circles show the results of Obayya et. al. [10]. The results agreed very well.

## 4.2    Modal Solution of Solid Core PCF under External Stress

A specific geometrical structure of a solid core PCF is chosen to carry out the study and analysis throughout this work. The chosen PCF is having four rings of air holes with hole diameter d=1.4 μm, pitch $\Lambda$=2.3 μm and over all diameter D=10.5 μm. The Fig. 4.8 shows the cross-section of the PCF under our study and analysis. For the structure, we apply external pressure uniformly

from all directions in the analysis. We carry out stress analysis, read the refractive indices, and use the new refractive indices to carry out optical analysis to find the fundamental mode. The effect of thermal stress as well as external stress is considered during the stress analysis. Thus the effect of uniform external stress on various properties of the PCF will be discussed in the subsequent sections of this chapter.
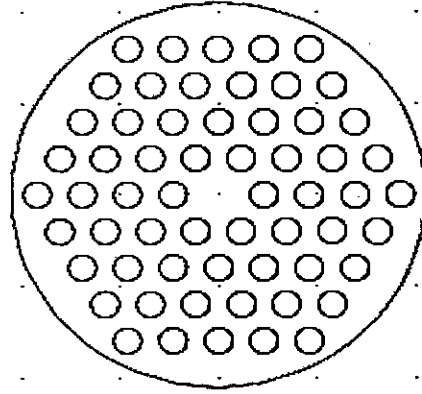


Fig. 4.8 : Schematic diagram of the cross section of the solid-core PCF with $\Lambda = 2.3$ µm, d = 1.4 µm, D = 10.50 µm.

Fig.4.9 shows the plot of the total displacement of the PCF, where Fig. 4.9(a) shows the vector plot of the displacement and Fig. 4.9(b) shows the contour plot of the displacement. From the contour plot it can be seen that there is strain all over the cross section of the PCF. The readings are obtained at wavelength $\lambda$=1.55 µm with external pressure 4GPa. From the plot it is observed that the maximum displacement = $7.335e^{-7}$ m. and the minimum displacement = $1.91e^{-9}$ m.
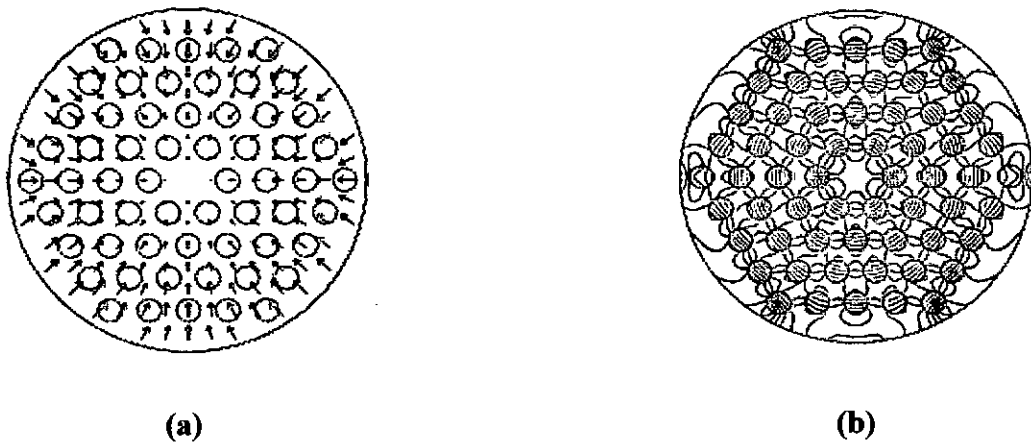


(a)                                                      (b)

Fig. 4.9: Total displacement in the four ring PCF  (a) vector plot (b) contour plot  under uniform external pressure P=4 GPa, $\lambda$=1.55 µm, $\Lambda = 2.3$ µm, d = 1.4 µm

The displacement diagram shown in Fig. 4.9 shows that there occurs uniform displacement throughout the cross section of the PCF due to the uniform force applied from all directions. This displacement causes change in the refractive index of the PCF material along the diameter of the PCF. The symmetric nature of the cross section plot of the $N_x$-$N_y$ shown in Fig. 4.10 explains the fact that due to uniform external pressure on the PCF, there occurs uniform displacement in the PCF material which, in turn, causes birefringence in the material. Also, the large change in index at silica-air interface is the reason of high birefringence in PCF under consideration. The further study shows that the birefringence increases with the increase of the external force.
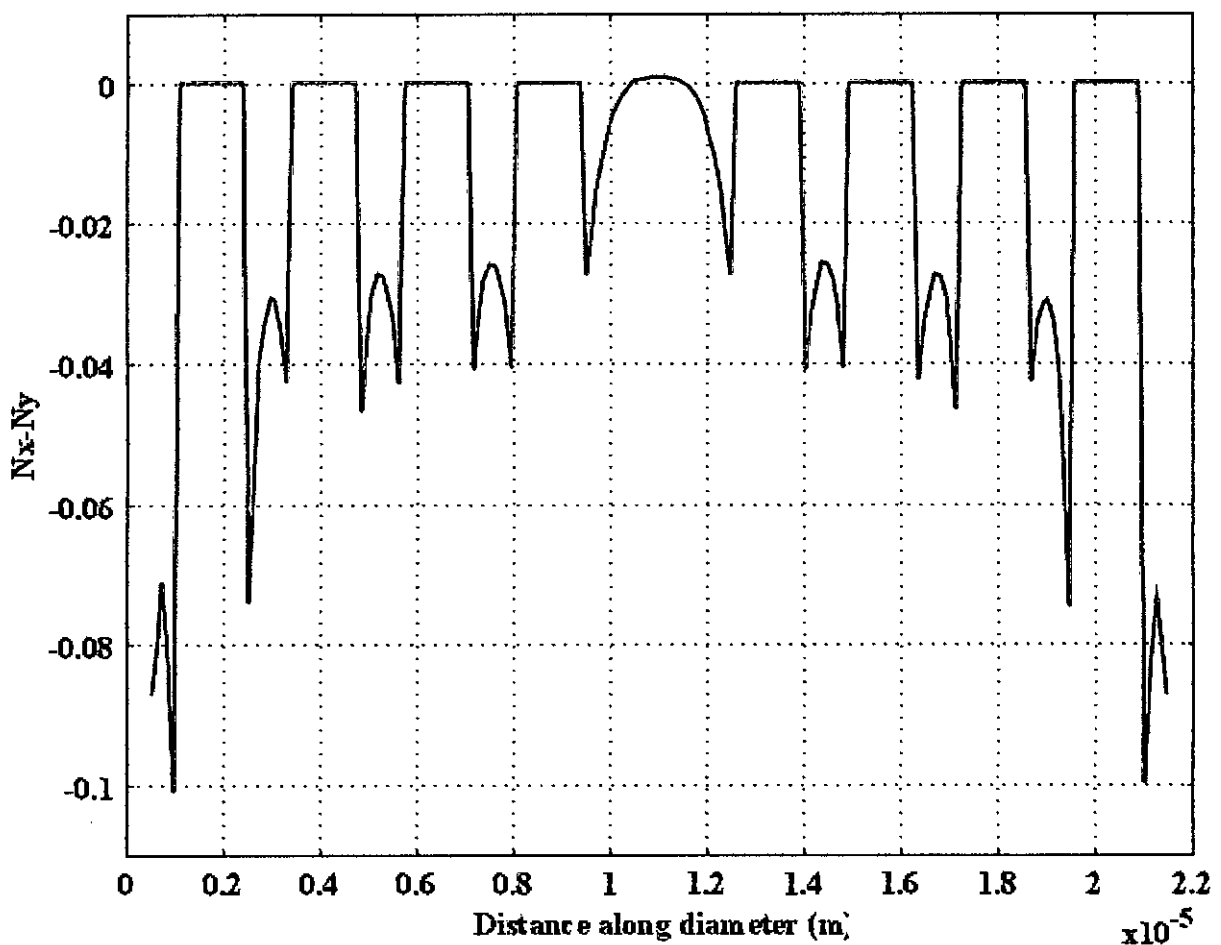


Fig. 4.10 :  Cross section plot of the $N_x$-$N_y$ in the solid-core PCF under uniform external pressure (d=1.4 μm, Λ=2.3 μm, λ=1.55 μm, external force P= 4 GPa)

As we have seen that due to the external stress the displacement over the cross section of the PCF changes uniformly, so are the cases with the refractive index and birefringence of the material of the PCF. The effect of stress on the refractive index also causes a change in the mode field distribution. For the fundamental $x$ polarized mode, $HE^x_{11}$ mode, we see the 3D and surface plot of the power flow as well as the corresponding electric and magnetic fields in Fig. 4.11.
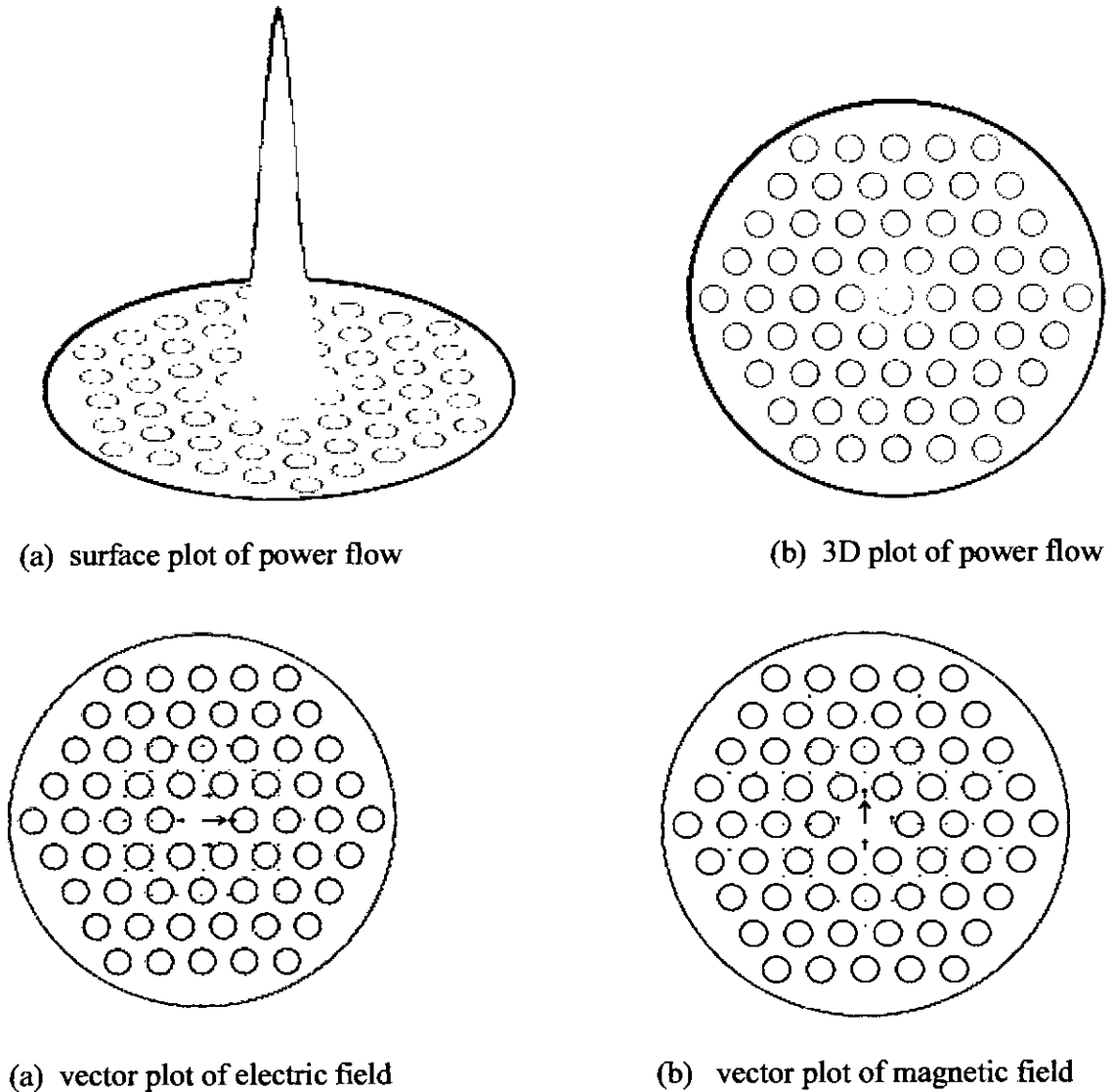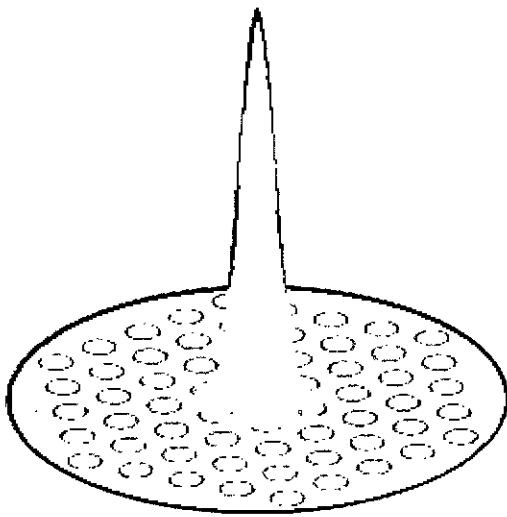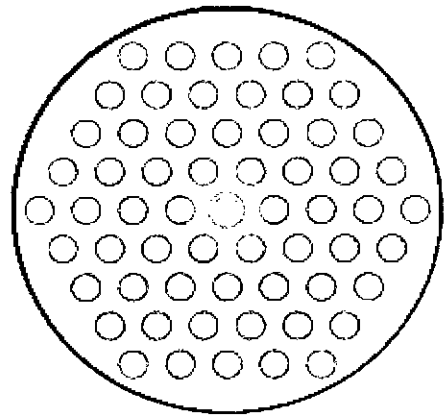


(a) surface plot of power flow

(b) 3D plot of power flow

(a) vector plot of electric field

(b) vector plot of magnetic field

Fig. 4.11 : Power flow (time average, z component) and corresponding electric and magnetic fields in a four ring PCF with d=1.4 μm, Λ=2.3 μm, λ=1.55 μm and P = 4 GPa for $x$-polarized mode.

From the plot it is observed that the maximum value the power flow is $2.097e^4$ W/m$^2$ and the minimum value is $-5.687e^{-12}$ W/m$^2$ at an external pressure P=4GPa with operating wavelength λ=1.55 μm.

For the fundamental $y$ polarized mode, $HE^y_{11}$ mode, we see the 3D and surface plot of the power flow as well as the corresponding electric and magnetic fields in Fig. 4.12. From the plot it is observed that the maximum value the power flow is $2.105e^4$ W/m$^2$ and the minimum value is - $6.721e^{-14}$ W/m$^2$ at an external pressure P=4GPa with operating wavelength $\lambda$=1.55 µm.
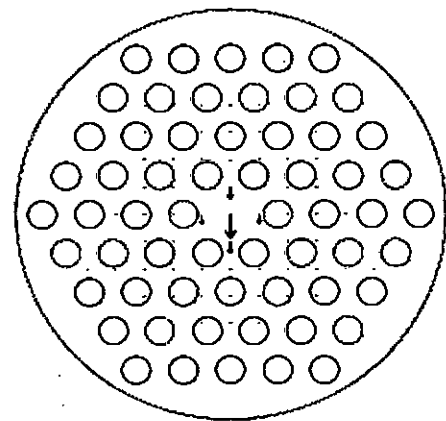


(a) 3D plot of power flow

(b)  surface plot of power flow
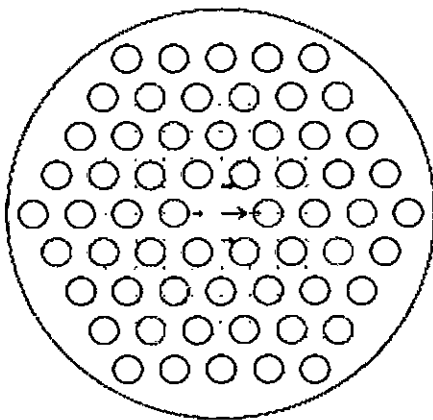


(c)  vector plot of electric field

(d)  vector plot of magnetic field

Fig. 4.12 :  plot of  (a) 3D plot of power flow, (b)  surface plot of power flow  (c) electric field (vector)  (d) magnetic field (vector) in a four ring PCF with force P= 4 GPa  ($y$-polarized mode)

## 4.3 Effect of Stress on Refractive Index and Birefringence

An unstressed (external pressure P=0) PCF is considered and the fundamental propagation mode is found at each value of the varying wave lengths. Thereafter, pressure is applied uniformly from all directions, and on reading the changed refractive index due to the applied stress, optical analysis is carried out to find the fundamental mode. The external stress acting on the holey fiber induces a specific stress distribution in the fiber's cross section. This stress distribution causes isotropic glass to become birefringent. The Fig. 4.13 shows the fact that the effective index, $n_{eff}$, over the operating frequency range (wavelength 0.7 μm – 2.0 μm) decreases almost linearly. It is also evident from the plot that at both fundamental modes $n_{eff}$ increases with the increase of external pressure.
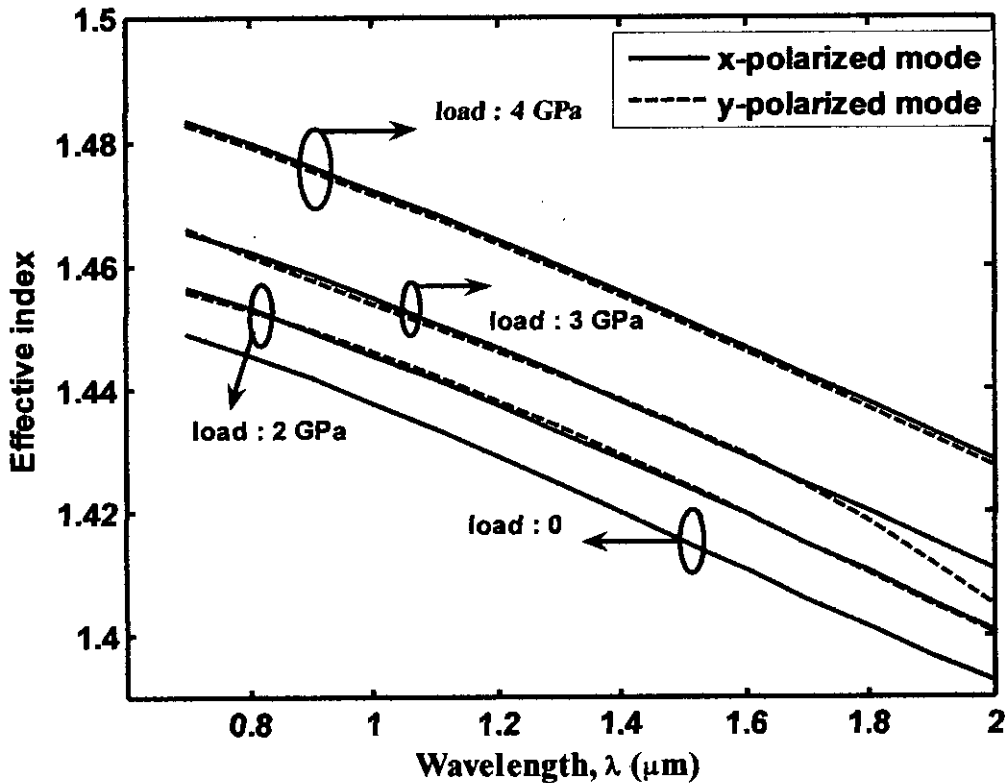


Fig. 4.13 : Effective index versus wavelength (four-ring PCF with d=1.4 μm, Λ=2.3 μm) at different external pressure conditions

As we know birefringence is the difference between the effective mode indices of two orthogonal polarization modes. The results show that the modal birefringence is negligible (of the order $10^{-5}$), and not shown in the figure when there is no external pressure (P=0). It is also revealed from the readings that birefringence remains almost flattened over the operating

55

wavelength range at external pressures 1, 2 and 4 GPa. On the other hand, birefringence increases remarkably with the increase of uniform external pressures which reaches of the order of $10^{-4}$. The relation between the phase birefringence and the effective index at different load conditions is shown in Fig. 4.14.
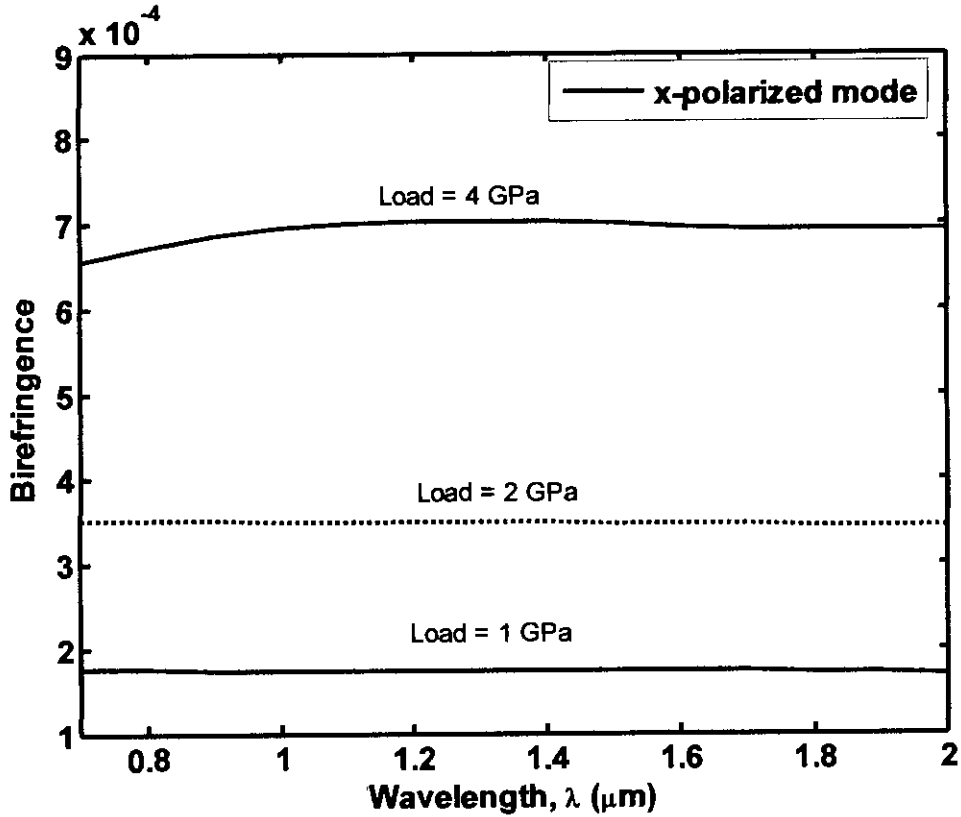


Fig. 4.14 : Phase birefringence versus wavelength (four-ring PCF with d=1.4 μm, Λ=2.3 μm) at different external pressure conditions

At zero pressure the modes are degenerate, but as load increases, the degeneracy gets lost and modal birefringence increases which become distinct at 4 GPa external pressure. In each experiment, effect of temperature (1000°c) has been taken into account. Here, Sellmeier equation has been used to include the material dispersion in calculation of modal effective index (refractive index) of fundamental modes in the calculations. The Sellmeier equation is shown below:

$$n^2 - 1 = \frac{A_1 \lambda^2}{\lambda^2 - \lambda_1^2} + \frac{A_2 \lambda^2}{\lambda^2 - \lambda_2^2} + \frac{A_3 \lambda^2}{\lambda^2 - \lambda_3^2} + \ldots\ldots\ldots\ldots \tag{4.1}$$

where, for silica (SiO$_2$) the values of the constants are:

**Table 4.1:** Values of the constants of the Sellmeier equation

| $A_1$ | 0.6961663 | $A_2$ | 0.4079426 | $A_3$ | 0.8974794 |
|---|---|---|---|---|---|
| $\lambda_1(\mu m)$ | 0.0684043 | $\lambda_2(\mu m)$ | 0.1162414 | $\lambda_3(\mu m)$ | 9.896161 |

The calculated values of refractive index of $SiO_2$ at the values of $\lambda$ used in the analysis are given below:

**Table 4.2:** Refractive indices of the PCF considering material dispersion (using Sellmeier equation)

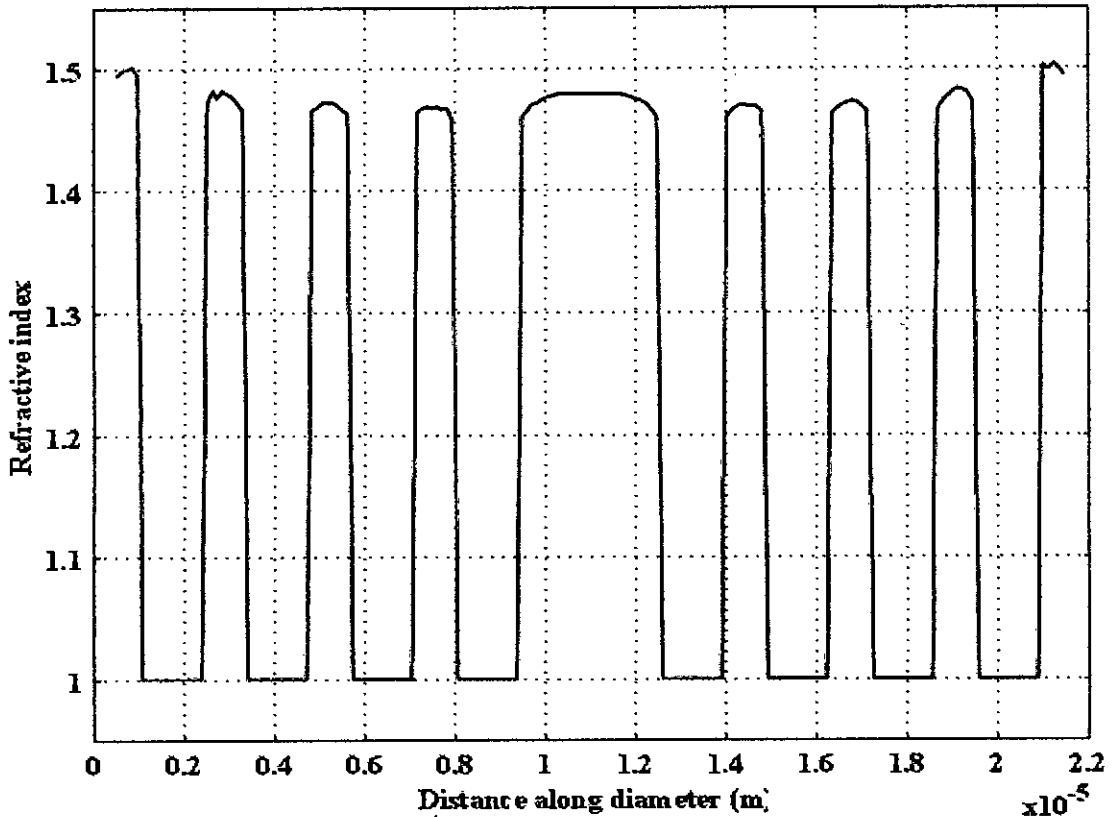| $\lambda$ ($\mu m$) | 0.6 | 0.7 | 0.8 | 0.9 | 1.0 | 1.1 | 1.2 | 1.3 | 1.4 |
|---|---|---|---|---|---|---|---|---|---|
| $n_{SiO2}$ | 1.4580 | 1.4553 | 1.4533 | 1.4517 | 1.4504 | 1.4492 | 1.4480 | 1.4469 | 1.4458 |
| $\lambda$ ($\mu m$) | 1.5 | 1.55 | 1.6 | 1.7 | 1.55 | 1.8 | 1.9 | 2.0 | |
| $n_{SiO2}$ | 1.4446 | 1.4440 | 1.4434 | 1.4422 | 1.4440 | 1.4400 | 1.4380 | 1.4370 | |



Fig.4.15 : Refractive index of the PCF due to applied stress (4 GPa) at $\lambda$= 1.550 $\mu m$

It is evident from the Fig.4.15 that the refractive index of the material (SiO2) of the PCF is changed due to application of the external stress. The change increases towards the edge of the fiber and reaches the highest value approximately 1.5 at the extreme edge. On the other hand, the stress can not affect the refractive index of the air holes (its value remains constant at 1.0). It is worth to mention here that the refractive index of silica has been assigned as 1.4440 as obtained using Sellmeier equation (Eq. 4.1) from Table 4.2 as input before carrying out the stress

57

analysis. FEMLAB uses this varying refractive index to determine the effective index, $n_{eff}$ of the PCF.

## 4.4 Effect of Stress on Group Birefringence

Now, to observe the variation of group birefringence, $B_g$ of the PCF under study at different operating wavelengths we have calculated the $B_g$ using Eq. (2.6) and plotted in the Fig. 4.16. The figure shows the group birefringence which is almost wavelength independent at '0' (zero) external load. But $B_g$ decreases almost linearly with the increase of the external stress over the operating wavelengths. In conventional fibers, the dependence of birefringence ($B$) on wavelength ($\lambda$) is almost negligible (which is obtained in our results at stress, P=0), so the group birefringence and the phase birefringence are almost the same. However, for the PCF under external stress, the change in phase birefringence ($B$) is higher due to the higher refractive index contrast, and the $2^{nd}$ term ($\lambda\dfrac{dB}{d\lambda}$) in Eq. (2.6) is also no longer negligible. Thus the group birefringence and the phase birefringence values are different.
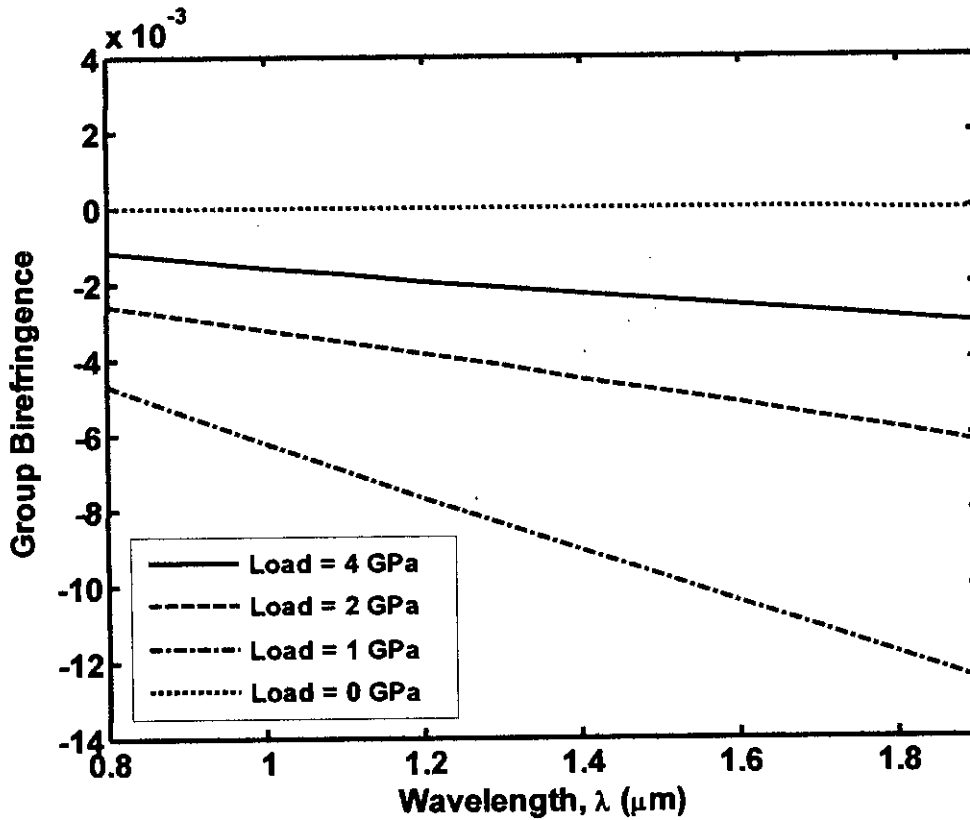


Fig. 4.16 : Group birefringence versus wavelength (four-ring PCF with d=1.4 μm, Λ=2.3 μm) at different external load conditions

## 4.5 Effect of Stress on Beat Length

In Fig. 4.17.(a) and (b) we have plotted the beat length $L_B$ against the wavelength at different external load situations for the PCF structure under our study. The beatlength has been calculated using the Eq. (2.10) as discussed in chapter 2. The calculated results exhibit that beat length increases almost linearly at low external pressure situation. But the rate of increment at higher external stress is higher over the operating wavelength. Obviously, this explains the higher change in the phase birefringence at higher applied external force.
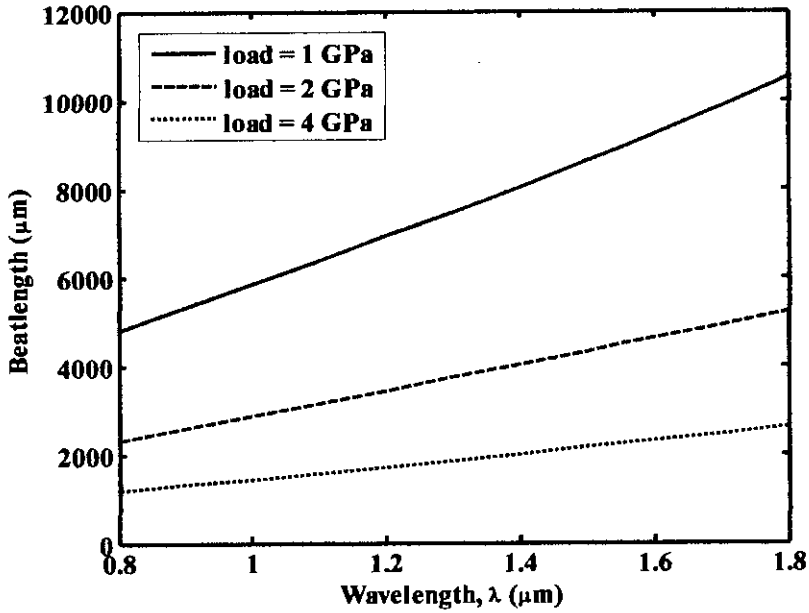


(a)
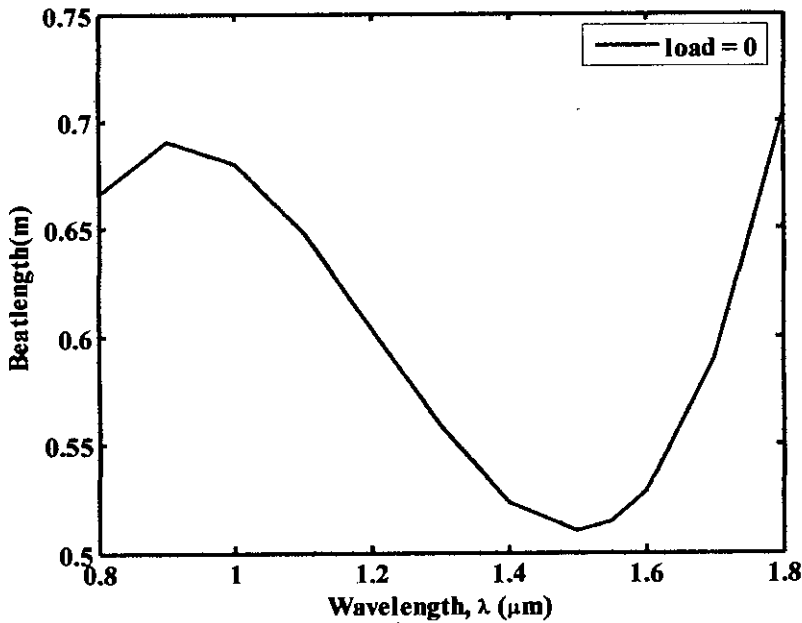


(b)

Fig. 4.17: Beat length versus wavelength (four-ring PCF with d=1.4 μm, Λ=2.3 μm) at no (zero) external pressure conditions

59

## 4.6    Effect of Stress on Effective Mode Area

The values of $A_{\textit{eff}}$ at different wavelengths under the effect of different external load situations have been calculated through FEM using Eq. (2.11) as discussed in chapter 2 and plotted in Fig. 4.18.    From the figure (Fig. 4.18) it is evident that $A_{\textit{eff}}$ increases almost linearly with the increase of operating wavelength irrespective of the value of the applied external stress (up to 4 GPa).    But, it is interesting to note that, the effective mode area, $A_{\textit{eff}}$ converses at the extreme end of the operating wavelength (2µm) at all values of the applied force.    However, at higher external pressure (4 GPa), the linearity of $A_{\textit{eff}}$ is lost at lower operating wavelength (upto 1µm). Here, Sellmeier equation has been used to include the material dispersion in the calculation of modal effective index (refractive index) of fundamental modes in the calculations.
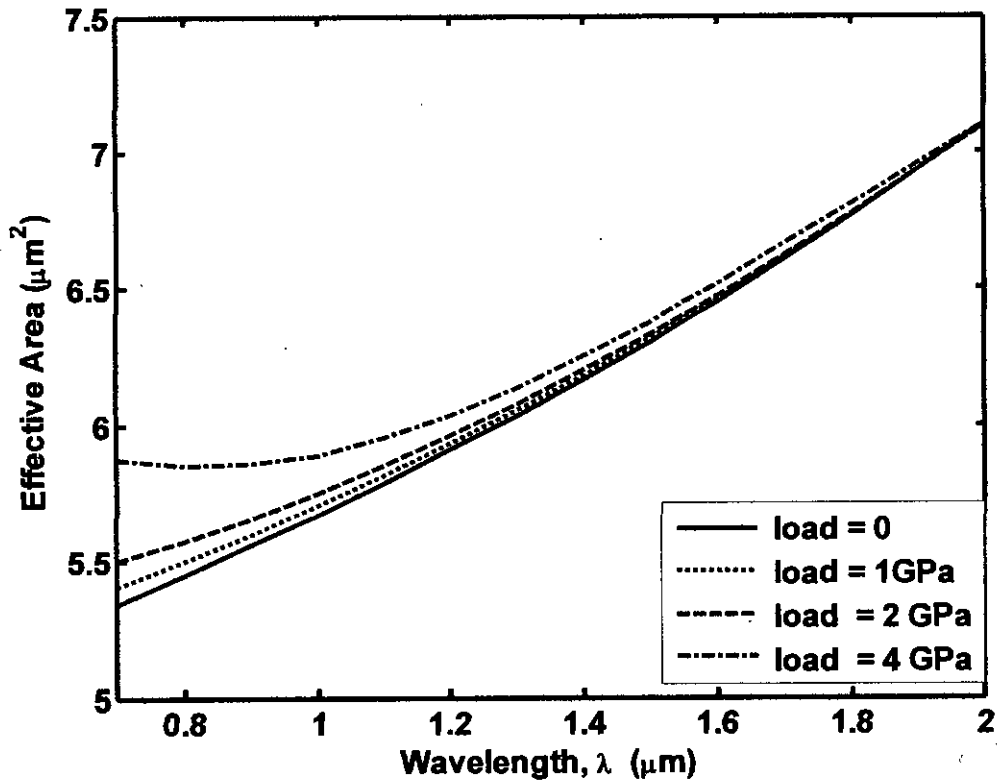


Fig. 4.18 : Effective mode area versus wavelength in a PCF (d=1.4 µm and Λ=2.3 µm) at different external stress situations

The Fig. 4.19 shows the effect of external stress on the effective mode area, $A_{eff}$ of PCFs with different number of air hole rings.
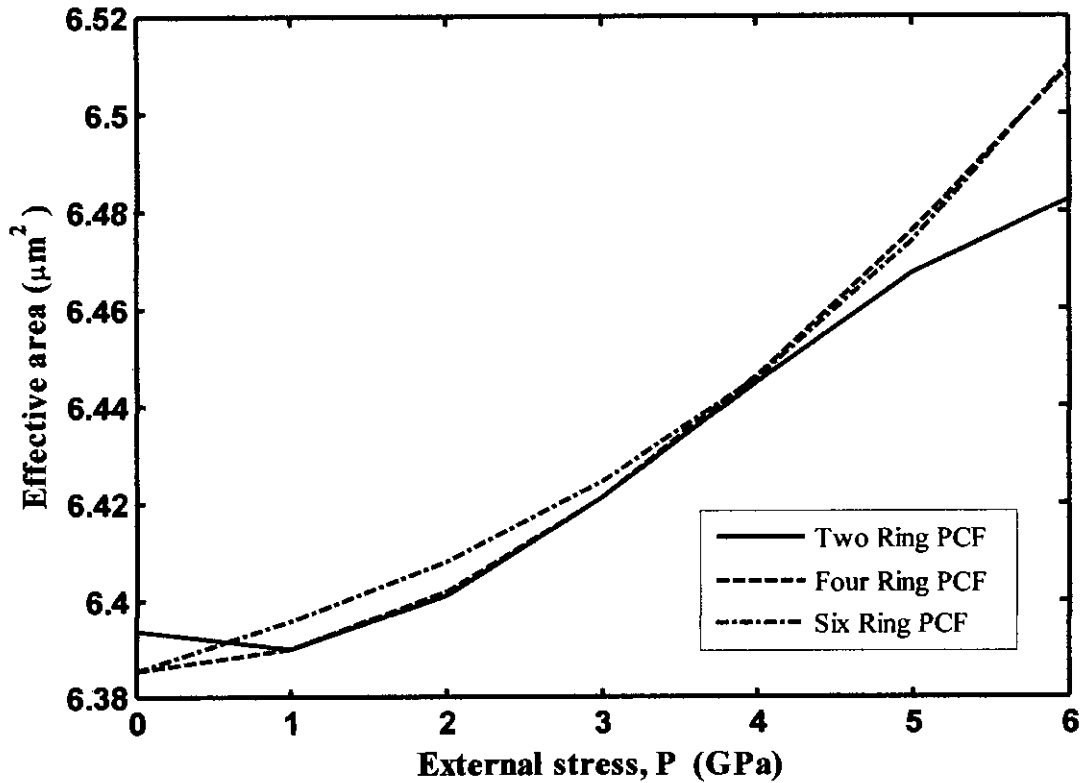


Fig. 4.19 : Effect of external stress on the effective mode area of PCFs (d=1.4 μm and Λ=2.3 μm, λ=1550 nm) with different geometry (number of air hole rings)

From Fig.4.19, it is revealed that the effective mode area, $A_{eff}$ increases with the application of external pressure. It is also evident that the effective mode area converses at external pressure 5 GPa and above for PCF structure with 4 and 6 air hole rings. This also justifies as to why we have taken for our research a PCF with 4 air hole rings. It is worth mentioning here that the relationship between effective mode area, $A_{eff}$ and geometry (air hole dia, pitch, etc) of PCF has been studied in [8]. But impact of external pressure on PCF of different geometry has not yet been reported upon. Thus, in this paper, what we believe that for the first time we are presenting a good study in this respect.

61

## 4.7 Effect of Stress on Polarization Mode Dispersion

Polarization mode dispersion (PMD), another source of limitation, occurs because although the single mode fiber can sustain only one transverse mode, it can carry this mode with two different polarization velocities for the two orthogonal polarization states, and slight imperfections or distortions in a fiber can alter the propagation velocities for the two orthogonally polarized waves. The external stress acting on the holey fiber induces a specific stress distribution in the fiber's cross section and also deformation of the fiber's structure. Both factors have an effect on the phase and the group modal birefringence, and therefore, affect the PMD of the PCF. In our work we have found the phase modal birefringence is positive, but the group birefringence (and, hence the PMD) is negative. This difference in sign between B and $B_g$ is caused by high anomalous chromatic dispersion of the phase modal birefringence (dB/d$\lambda$ > 0) [20].

The PMD (measured in ps-km$^{-1}$) is expressed in terms of group delay, $G_d$ and calculated using Eq. 2.16 as explained in chapter 2. The PMD can also be calculated in terms of the group birefringence, $B_g$ as shown in Eq.2.16 [20]. The Fig. 4.20 depicts the variation of the PMD with the operating wavelength, $\lambda$ at different external stress conditions. As the group birefringence is almost $\lambda$ independent at `0' (zero) external load, and its value is too low; so is the value of PMD (PMD, $\tau_g = \dfrac{B_g}{c}$). As such it is not shown here. From the figure it is evident that PMD decreases almost linearly with the increase of the wavelength. But it is interesting to observe that the rate of decrease of the PMD is higher at higher external pressure.
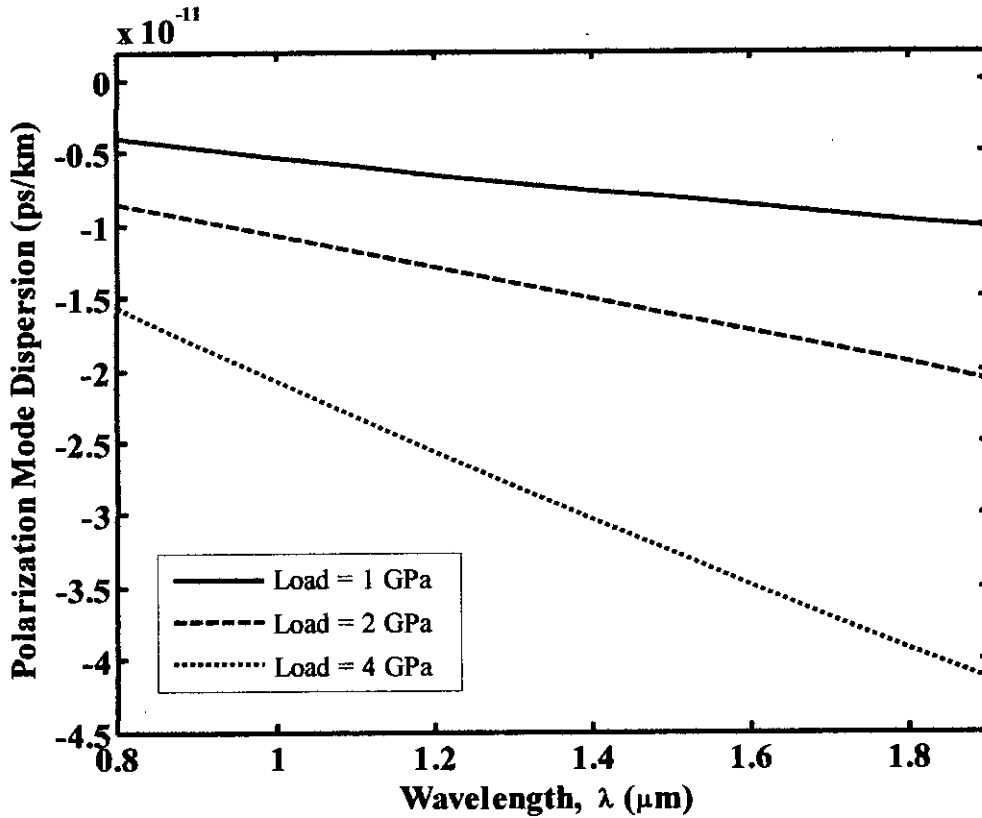
Fig. 4.20 : Variation of PMD in the four ring  PCF (d=1.4 μm and  Λ=2.3 μm) at various external pressure conditions taking wavelength, λ as parameter

## 4.8   Effect of External Stress on Dispersion

In single-mode, fiber performance is primarily limited by chromatic dispersion (also called group velocity dispersion), which occurs because the refractive index of the glass material varies slightly depending on the wavelength of the light, and light from real optical transmitters necessarily has nonzero spectral width (due to modulation)[29].   PCFs possess the attractive property of great controllability in chromatic dispersion [4]-[12].   The chromatic dispersion profile can be easily controlled by varying the hole diameter, d and the hole pitch, Λ   For practical applications to optical communication systems, dispersion compensations, and nonlinear optics, controllability of chromatic dispersion in PCFs is a critical issue. So far, various PCFs with significant dispersion properties have been studied and reported in  [7]-[15].  But how do these properties of PCF get affected with the application of external pressure still remains

unaddressed. In this work, we have carried out detail study on the dispersion property of PCF under external pressure while taking into consideration the stress due to thermal effects. The working equation to calculate dispersion in PCF can be re-written as

$$D = -3333.3\left[\lambda\frac{d^2 n_{eff}}{d\lambda^2}\right] \text{ ps/(nm.km)} \tag{4.1}$$



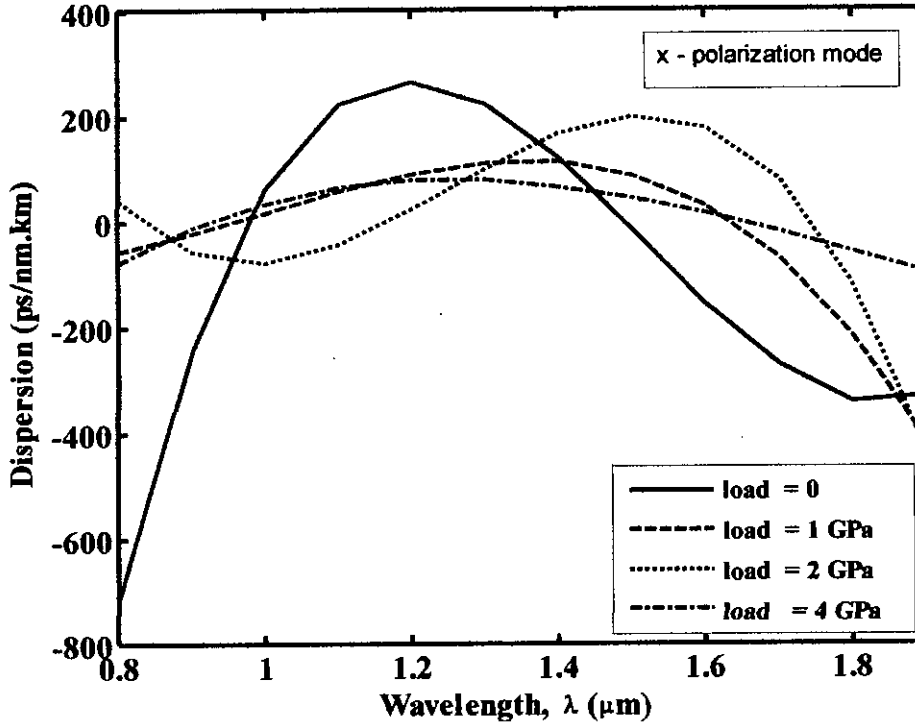Fig. 4.21 : Variation of dispersion in PCF (d=1.4 μm and Λ=2.3 μm) with λ at different external load condition (x-polarization mode)
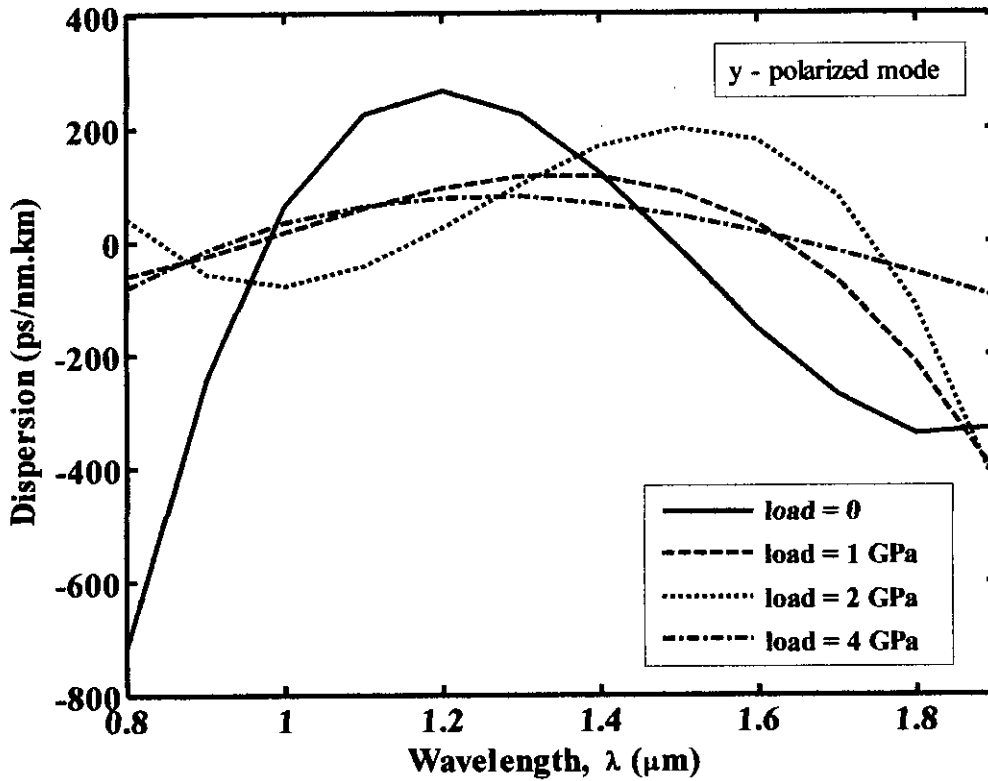
Fig. 4.22 : Variation of dispersion in PCF (d=1.4 μm and Λ=2.3 μm) with λ at different external load condition (y-polarization mode)

We have calculated the dispersion at various wavelengths and with variation of external applied force up to 4GPa. The graph shows that a flattened dispersion curve is possible at an external applied load of 2GPa over the wide operating wavelength. But at zero external load (P=0), the dispersion in the PCF shows anomalous reading which conforms to the results of normal PCF. PCFs at higher applied external pressure (4GPa, in this case), the dispersion again shows some anomalous readings. Thus it reveals that at specific value of external pressure the material of the PCF exhibits specific dispersion values. Thus, the PCF has got tremendous potential to be used as dispersion compensator devices in the field of telecommunications and other fields of applications.

# CHAPTER 5

# Conclusion

## 5.1   Conclusion of the work

In this work, study and analysis have been done to evaluate various propagation properties of photonic crystal fibers considering thermal and external stress effects. The finite element method (FEM) has been applied to carryout the modal solution of the PCFs. COMSOL Multiphysics has been employed as a modeling tool, where a combination of structural mechanics module and electromagnetic module has been used to carry out the stress analysis and optical mode analysis of the PCF, respectively. In this work, the external stress is applied from all directions, which occurs uniform displacement throughout the cross section of the PCF and the refractive index of the PCF material changes and becomes anisotropic due to the stress-optic effect. Then the vector finite element method (FEM) is used for modal analysis to find the effective index and field solutions, which is used to find modal birefringence, beat length, group birefringence, effective mode area, polarization mode dispersion, group velocity dispersion, etc. for two fundamental orthogonal modes.

It is observed that due to the external stress the phase birefringence increases significantly (of the order of $10^{-3}$). As the phase birefringence increases with the increase in external stress over a wide operating wavelength (up to 2µm), the beat length decreases. However, the group birefringence of the PCF decreases almost linearly with the increase in the external stress over the operating wavelengths. The difference in sign between phase birefringence (+ve) and group birefringence (-ve) is caused by high anomalous chromatic dispersion of the phase modal birefringence. It is seen that the effective mode area increases almost linearly with the increase of external pressure. In this work, it is also observed that the group birefringence decreases with the increase of external stress, and hence, the PMD also decreases almost linearly with the increase of the external stress over a wide operating wavelength. It is revealed from the result that flattened dispersion curve could be possible over the wide operating wavelength even under external stress. But at zero external load, the PCF shows highly anomalous dispersion. Also, PCFs at specific external stress, show specific dispersion pattern. Thus, the fact remains valid that PCFs possess the attractive property of great controllability in chromatic dispersion.

## 5.2   Recommendations for Future Works

Highly birefringent photonic crystal fibers may be designed by creating asymmetries in the geometric structure (changing air hole diameter, pitch length etc.) of the PCF and efforts may be taken to study and analyze the effects of external stress on this type of asymmetric PCFs. Effects of external stress on the properties of other types of PCF, the Photonic Bandgap Fiber (PBF), for example, need to be investigated. Research should be continued to find PCFs with different structures which can also withstand higher external stress. Research should also be extended to find more suitable, accurate and user friendly numerical analysis method and simulation software for carrying out stress and optical analysis of PCFs in the days to come.

# REFERENCES

[1] Russel, P. St. J, "Photonic crystal fibers," *Science*, vol.299, pp. 358-362, Jan. 2003.

[2] Knight, J.C., "Photonic crystal fibers," *Nature,* vol. 424, pp.847-851, 14 Aug. 2003.

[3] Russel, P. St. J., "Photonic crystal fibres: A historical account" *www.PCFIBER.Com*, October 2007..

[4] Birks, T., Knight, J., and Russel, P. St. J, "Endlessly single mode photonic crystal fiber," *Opt. Lett.*, vol. 22, no. 13, pp.961-963, July 1999.

[5] Zolla, F., Reneversez, G., Nicolet, A., Kuhlmey, B., Guenneau, S., and Felbacq, D., " Foundation of photonic crystal fibers," *1st edition, Imperial College Press*, 2005.

[6] Bjarklev, A., Broeng, J., and Bjarklev, A. S., "Photonic crystal fibers", *Kluwer Academic Publishers*, © 2003 Springer Science + Business Media, Inc, USA, 2003.

[7] Koshiba, M., "Full-vector analysis of photonic crystal fibers using the Finite Element Method," *ICECE Trans. Electron.*, vol. E85-C, no.4, pp.881-888, Apr. 2002.

[8] Saitoh, K., and Koshiba, M., "Numerical modeling of photonic crystal fibers," *J. of Light wave technol.* vol. 23, No.11, pp. 3580-3590, Nov. 2005.

[9] Alam, M.S., Saitoh, K., and Koshiba, M., "High group birefringence in air-core photonic crystal fibers," *Opt. Lett.*, vol. 30, no.8, pp. 824-826, 15 Apr. 2005.

[10] Obayya, S.S.A., Rahman, B.M.A., and Grattan, K.T.V., "Accurate finite element modal solution of photonic crystal fibers," *IEEE Proc-Optoelectron.*, vol.152, no. 5 pp.241-246, Oct. 2005.

[11] Zhang, F., Zhang, M., Liu, X., and Ye, O., "Design of wideband single-polarization single- mode photonic crystal fiber," *J. of light wave technol.*, vol.25, no.5, pp.1184-1189, May 2007.

[12] Ademgil, H., and Haxha, S., "Highly birefringent photonic crystal fibers with ultra low chromatic dispersion and low confinement losses," *J. of Light wave technol.*, vol.26, no.4, pp.441-448, Feb. 2008.

[13] Abdur Razzak, S. M., and Namihira, Y., "Tailoring dispersion and confinement losses of photonic crystal fibers using a hybrid cladding," *J. of Light wave technol.*, vol.26, no.13, pp.1909-1914, July 2008.

[14] Okamoto, K., "Fundamentals of optical waveguides," *Academic press*, 2000.

[15] Guan, N., Habu, S., Takenaga, K., Himeno, K. and. Wada, A. "Boundary element method for analysis of holey optical fibers" *J. Light wave technol*, vol.21. pp. 1787-1792, Aug. 2003.

[16]. Zhu, Z., and Brown, T.G., ''Full-victor finite difference analysis of microstructured optical fibers'', *Optics Express*, vol.10, no.17, pp.853-864, Aug 2002.

[17] Suzuki, K., Kubuta. H., Kawanishi, S., Tanka, M and Fujita, M., "Optical properties of a low-loss polarization maintaining photonic crystal fiber". vol.9, no.13/ *OPTICS EXPRESS*. pp. 676, Dec. 2001.

[18] Russel, P. St. J, "Photonic crystal fibers", *J. Light wave, technol* vol. 24, no. 12, pp. 4729 – 4749, 2006.

[19] Tian, H., Yu, Z., Han, L., and Liu, Y., "Birefringence and confinement loss properties in photonic crystal fibers under lateral stress," *IEEE Photon. Technol. lett.*, vol.20, no. 22, 15 Nov. 2008.

[20] Szpulak, M., Martynkien, T., Urbanczyk, W., "Effects of hydrostatic pressure on phase and group modal birefringence in micro-structured holey fibers" *Applied Optics*, vol. 43, no. 24, pp.4739-4744, 20 Aug 2004.

[21] Senior, M. J., "Optical fiber communications – principles and practices" 2nd edition, *Prentice-Hall of India Private Limited*, 2005.

[22] Agrawal, G., P. "Fiber-optic communication systems", third edition, *a John Wiley & Sons, Inc Publication*, 2005.

[23] Knight, J.C., Birks, T.A., Russell, P. St. J., and Atkin, D.M.: 'All-silica single-mode optical fiber with photonic crystal cladding', *Opt. Lett.*, vol. 21, pp.1547-1549, 1996.

[24] Knight, J.C., Birks, T. A., Cregan, R. F., Russell, P. St., J., and de Sandro, J.P.: 'Large mode area photonic crystal fiber', *Electron. Lett.*, vol. 34, pp.1347-1348, 1998.

[25] Gander, M.J., McBride, R., Jones, J. D.C., Mogilevtsev, D., Birks, T.A., Knight, J.C., and Russell, P. St. J: 'Experimental measurement of group velocity in photonic crystal fiber", *Electron. Lett.*, vol. 35, pp. 63-64, 1998.

[26] Cucinotta, A., Selleri, S., Vincetti, L., and Zoboli, M.: 'Holey fiber analysis through the finite element method', *IEEE Photonics technol. Lett.*, vol. 14, pp. 1530-1532, 2002.

[27] Saitoh, K., and Koshiba, M.: 'Chromatic dispersion control in photonic crystal fibers: application to ultra –flattened dispersion', *Opt. Express*, vol. 11, pp. 843-852, 2003.

[28] Photonic crystal fiber - *http://en.wikipedia.org/wiki/photonic-crystal_fiber*

[29] Solitons - *http://en.wikipedia.org/wiki/soliton*

[30] Ramo. S., 'Fields and waves in communication electronics', *John Wiley & Sons*.

[31] COMSOL Multyphysics, version 3.2a, September 2005.

69